Cerebral Cortex, May 2021;31: 2382–2401

doi: 10.1093/cercor/bhaa359
Advance Access Publication Date: 22 December 2020
Original Article

ORIGINAL ARTICLE

The Entorhinal Cortical Alvear Pathway Differentially Excites Pyramidal Cells and Interneuron Subtypes in Hippocampal CA1

Karen A. Bell, Rayne Delong, Priyodarshan Goswamee and A. Rory McQuiston

Department of Anatomy and Neurobiology, Virginia Commonwealth University School of Medicine, Richmond, VA 23298, USA

Address correspondence to A. Rory McQuiston, Department of Anatomy and Neurobiology, Virginia Commonwealth University School of Medicine, Box 980709, Richmond, VA 23298, USA. Email: amcquiston@vcu.edu.

Abstract

The entorhinal cortex alvear pathway is a major excitatory input to hippocampal CA1, yet nothing is known about its physiological impact. We investigated the alvear pathway projection and innervation of neurons in CA1 using optogenetics and whole cell patch clamp methods in transgenic mouse brain slices. Using this approach, we show that the medial entorhinal cortical alvear inputs onto CA1 pyramidal cells (PCs) and interneurons with cell bodies located in stratum oriens were monosynaptic, had low release probability, and were mediated by glutamate receptors. Optogenetic theta burst stimulation was unable to elicit suprathreshold activation of CA1 PCs but was capable of activating CA1 interneurons. However, different subtypes of interneurons were not equally affected. Higher burst action potential frequencies were observed in parvalbumin-expressing interneurons relative to vasoactive-intestinal peptide-expressing or a subset of oriens lacunosum-moleculare (O-LM) interneurons. Furthermore, alvear excitatory synaptic responses were observed in greater than 70% of PV and VIP interneurons and less than 20% of O-LM cells. Finally, greater than 50% of theta burst-driven inhibitory postsynaptic current amplitudes in CA1 PCs were inhibited by optogenetic suppression of PV interneurons. Therefore, our data suggest that the alvear pathway primarily affects hippocampal CA1 function through feedforward inhibition of select interneuron subtypes.

Key words: brain slice, optogenetics, synapse, theta burst, whole cell patch clamping

The hippocampus receives the majority of its excitatory input from the entorhinal cortex (EC). The EC projects to hippocampal CA1 via two converging pathways. One is the temporo-ammonic (TA) pathway that perforates the subiculum and courses through the stratum lacunosum-moleculare (SLM) to synapse on CA1 pyramidal cell (PC) and interneuron dendrites located in the SLM (Steward 1976; Steward and Scoville 1976). The other is the alvear pathway that courses through the alveus and adjacent stratum oriens (SO) of hippocampal CA1. After coursing transversely through the alveus, EC axons of the alvear pathway turn to ascend through all layers of hippocampal CA1 to terminate on PC and interneuron dendrites in the SLM (Deller et al. 1996). Although the alvear pathway ultimately terminates in the SLM, alvear pathway axons in the SO have synaptic boutons that are thought to form excitatory synaptic connections with CA1 PC and interneuron dendrites (Deller et al. 1996). However, the physiological impact of the synapses in the SO has not been investigated.

It is well known that the EC and hippocampus have crucial roles in the formation of long-term memories. In rodent, the alvear pathway carries most of the entorhinal input to dorsal hippocampal CA1 (Deller et al. 1996). In humans, the alvear pathway also plays a prominent role in relaying inputs from the EC to hippocampal CA1 (Zeineh et al. 2017). Despite the

significance of the alvear pathway, the physiological effect of the alvear pathway on the postsynaptic neurons and network function of hippocampal CA1 has not, to our knowledge, been reported. This is in spite of the extensive knowledge of the effect of in vivo EC stimulation on the excitability of hippocampal CA1. Some groups have observed a monosynaptic suprathreshold activation of CA1 PCs following electrical stimulation of the EC in vivo (Segal 1972; Yeckel and Berger 1990, 1995), whereas other groups observed only subthreshold events (Andersen et al. 1966; Leung et al. 1995).

In contrast, ex vivo studies have demonstrated that the primary effect of stimulating hippocampal CA1 TA inputs (Empson and Heinemann 1995a, 1995b) or all afferents in the SLM (including the TA, alvear, and thalamic nucleus reuniens pathways) is feedforward inhibition of hippocampal CA1 PCs (Colbert and Levy 1992; Dvorak-Carbone and Schuman 1999; Ang et al. 2005). Notably, it appears that specific subsets of interneurons can be potently activated by SLM excitatory inputs, whereas others are only weakly affected or not affected at all (Milstein et al. 2015). However, the alvear inputs are in an anatomical distinct position to engage unique groups of interneurons in hippocampal CA1 and may have a differential effect on hippocampal network function relative to the TA input. To explore this, we expressed the optogenetic excitatory channel oChIEF (Lin et al. 2009) in layers 2 and 3 (L2 and L3) of medial entorhinal cortex (MEC) to study the impact of these inputs onto PCs and interneurons with cell bodies located in the SO of hippocampal CA1. The MEC was chosen as the viral expression target by virtue of the transgenic mice available (see Materials and Methods). We found that activation of the alvear pathway produced subthreshold excitatory postsynaptic potentials (EPSPs) in CA1 PCs. In contrast, alvear pathway stimulation resulted in suprathreshold excitation of CA1 interneurons, which in turn produced $GABA_A$ inhibitory postsynaptic responses in CA1 PCs. A significant proportion of the interneurons activated by the alvear pathway were parvalbumin (PV)-expressing perisomatic interneurons that have been previously reported to have limited responses to TA pathway stimulation (Milstein et al. 2015). Therefore, our data suggest that, relative to the TA pathway, the alvear pathway can engage different hippocampal CA1 interneuron networks and may contribute to the generation of rhythms and perisomatic inhibition in hippocampal CA1.

Materials and Methods

Animals

NOP-tTA (B6.Cg-Tg(Klk8-tTA)QMmay/MullMmmh, MMRRC Stock No. 031780-MU) (Yasuda and Mayford 2006), pOXR-1-Cre (C57BL/6N-Tg(Oxr1-cre)C14Stl/J, JAX Stock No. 030484) (Suh et al. 2011), VIP-cre (*Vip*$^{tm1(cre)Zjh}$/J, JAX Stock No. 010908) (Taniguchi et al. 2011), PV-Cre (B6;129P2-*Pvalb*$^{tm1(cre)Arbr}$/J, Jax Stock No. 008069) (Hippenmeyer et al. 2005), PV-tdTomato (C57BL/6-Tg(Pvalb-tdTomato)15Gfng/J, JAX No. 027395) (Kaiser et al. 2016), GIN (FVB-Tg(GadGFP)45704Swn/J) (Oliva et al. 2000), Arch-GFP (B6;129S-*Gt(ROSA)26Sor*$^{tm35.1(CAG-aop3/GFP)Hze}$/J, Jax Stock No. 012735) (Chow et al. 2010), and TRE-oChIEF-Citrine (Cheetham et al. 2016) mouse lines used in these studies are outlined in Table 1. These mice were housed in an animal care facility approved by the American Association for the Accreditation of Laboratory Animal Care. Experimental procedures followed the protocol approved by the Institutional Animal Care and Use Committee of Virginia Commonwealth University (AD20205). This protocol adhered to the ethical guidelines described in the Guide for the Care and Use of Laboratory Animals 8th Edition (Council NR 2011). All efforts were made to minimize animal suffering and to reduce the number of animals used.

Breeding strategies

To examine medial entorhinal cortex inputs to hippocampal CA1, we expressed the excitatory optogenetic channel oChIEF-mCitrine (Lin et al. 2009) in L2/L3 MEC projection neurons using two different approaches. In the first approach, we injected the right hemisphere MEC of pOXR1-Cre mice (Suh et al. 2011) with an AAV that expressed oChIEF-mCitrine in a Cre-dependent manner (rAAV-hSyn-Flex-oChIEF-mCitrine) (Table 1 top, first two columns). The pOXR1-Cre line confined expression of oChIEF-mCitrine primarily to L3 MEC projection neurons (Suh et al. 2011). In the second approach, we crossed the tTA-driver mouse line NOP-tTA (Yasuda and Mayford 2006) with a tTA reporter mouse line TRE-oChIEF-Citrine (Cheetham et al. 2016) to produce NOP-tTA;TRE-ChIEF-Citrine mice (Table 1 bottom, first two columns). This cross resulted in expression of oChIEF-mCitrine in layer 2 and L3 MEC projection neurons. We also expressed tdTomato or GFP selectively in interneuron subclasses to target interneuron subtypes for whole cell patch clamp recordings in hippocampal CA1 brain slices (Table 1, third column). To target PV interneurons, we crossed NOP-tTA;tetO-ChIEF-Citrine or pOXR1-Cre mice with either a homozygous cross of PV-Cre (Hippenmeyer et al. 2005) and Ai14 (tdTomato reporter) or a PV interneuron tdTomato expressing transgenic mouse line (PV-tdTomato) (Kaiser et al. 2016). To target VIP interneurons, we crossed NOP-tTA;tetO-ChIEF-Citrine or pOXR1-Cre mice with a homozygous cross of VIP-Cre (Taniguchi et al. 2011) and Ai14. Finally, we crossed NOP-tTA;tetO-ChIEF-Citrine or pOXR1-Cre mice with GIN mice that express GFP in a subset of somatostatin-expressing (SST) oriens lacunosum-moleculare (O-LM) interneurons (Oliva Jr. et al. 2000). To silence PV interneurons, we crossed NOP-tTA;tetO-ChIEF-Citrine or pOXR1-Cre mice with a homozygous cross of PV-Cre and Ai35D, a Cre-dependent reporter mouse line that expresses archaerhodopsin-GFP (Arch-GFP).

Stereotaxic injection of rAAV-hSyn-Flex-oChIEF-mCitrine into the MEC of pOXR1-Cre mice

To express oChIEF-mCitrine in pOXR1-Cre mice, a recombinant adeno-associated virus (rAAV, serotype 1, 4.8×10^{13} VC/mL titer) expressing FLEXed oChIEF-mCitrine (Addgene #50973) was package by Vector Biolabs (Malvern, PA). Mice were initially anesthetized via intraperitoneal injection of ketamine (100 mg/kg IP) and xylazine (2.5 mg/kg IP). Anesthesia was maintained with O_2 supplemented with 1.0% isoflurane. For injections into the right MEC, an incision was made in the skin along the midsagittal suture, and a small hole was drilled in the skull overlying the MEC. An aluminosilicate glass pipette containing rAAV-hSyn-Flex-oChIEF-mCitrine was lowered to the level of the MEC and infused at a rate of 100 nl/min using a software-driven injectomate (Neurostar, Sindelfingen, Germany). In total, 4×100 nL injections into the right MEC were made at AP = 300 µM rostral to the transverse sinus, ML = 3.2, and DV 4.0 to 3.55 mm. 21–28 days postviral injection, 61–105-day-old mice were sacrificed for experimentation. Of the 51 pOXR-1-Cre mice injected, the injection site was completely

Table 1 Mouse crosses used for AAV-driven MEC expression of oChIEF-mCitrine and tdTomato fluorescent labeling of select interneuron subtypes

MEC driver mouse line	AAV injected into MEC or reporter oChIEF mouse line	Interneuron driver mouse line	Cre-tdTomato reporter interneuron mouse line for Cre-driver line crosses
pOXR1-Cre	rAAV-hSyn-Flex-oChIEF-mCitrine	PV-Cre (Jax #008069, B6;129P2-*Pvalb*$^{tm1(cre)Arbr}$/J) PV-tdTomato (C57BL/6-Tg(Pvalb-tdTomato)15Gfng/J, JAX No. 027395) VIP-Cre (Jax # 010908, *Vip*$^{tm1(cre)Zjh}$/J) GIN (Jax # 003718, FVB-Tg(GadGFP)45704Swn/J	Ai14 tdTomato reporter mice (Jax # 007914, B6.Cg-Gt(ROSA)26Sortm14(CAG-tdTomato)Hze/J)
NOP-tTA	TRE-oChIEF-mCitrine	PV-Cre (Jax #008069, B6;129P2-*Pvalb*$^{tm1(cre)Arbr}$/J) PV-tdTomato (C57BL/6-Tg(Pvalb-tdTomato)15Gfng/J, JAX No. 027395) VIP-Cre (Jax # 010908, *Vip*$^{tm1(cre)Zjh}$/J) GIN (Jax # 003718, FVB-Tg(GadGFP)45704Swn/J	Ai14 tdTomato reporter mice (Jax # 007914, B6.Cg-Gt(ROSA)26Sortm14(CAG-tdTomato)Hze/J) Arch-GFP reporter mice (Jax # 012735, B6;129S-*Gt(ROSA)26Sor*$^{tm35.1(CAG-aop3/GFP)Hze}$/J)

missed in 3 animals and in 7 others no response could be observed in any of the neurons from which we recorded.

Preparation of hippocampal slices

Brain slices were obtained by methods previously described (Bell et al. 2011). Mice were anesthetized with an intraperitoneal injection of ketamine (200 mg/kg) and xylazine (20 mg/kg). Mice were transcardially perfused with ice cold saline (consisting of [in mM]: sucrose 230, KCl 2.5, CaCl 2, $MgCl_2$ 6, $NaHPO_4$ 1, $NaHCO_3$ 25, glucose 25) and sacrificed by decapitation. The brain was removed, hemi-sected, and horizontal slices containing the mid temporal hippocampus were cut at 350 µm on a Leica VT1200 (Leica Microsystems). Sections were incubated in a holding chamber kept at 32 °C. The holding chamber solution consisted of normal saline (in mM): NaCl 125, KCl 3.0, CaCl 1.2, $MgCl_2$ 1.2, $NaHPO_4$ 1.2, $NaHCO_3$ 25, glucose 25 bubbled with 95% O_2/5% CO_2. Recordings were performed at 32–35 °C.

Light-evoked release of glutamate from MEC axon terminals and light-evoked silencing of CA1 interneuron subtype populations

MEC terminals expressing oChIEF-mCitrine were stimulated by blue light and interneurons expressing Arch-GFP were hyperpolarized by orange light. Both light paths were transmitted through the epi-illumination light path of an Olympus BX51WI microscope (Olympus) and a 20× water immersion objective (0.95 NA). The objective was placed so that light illuminated the strata pyramidale and oriens and adjacent temporal associational cortex or lateral ventricle. No light was delivered to the strata radiatum or lacunosum-moleculare (Fig. 1A). Blue light flashes (0.1 ms in duration, 7.8 mW/mm^2) and orange light pulses (3 s in duration, 0.44 mW/mm^2) were generated from light-emitting diodes (LEDs) (UHP-microscope-LED-460 or UHP-T-LED-White filtered by an HQ 605/50× excitation filter, respectively, Prizmatix Modiin-Ilite, Givat Shmuel, Israel). These were the lowest light intensities that produced the maximum synaptic response in postsynaptic neurons (blue light) or the maximum hyperpolarization in interneurons expressing Arch-GFP (orange light). Blue or orange light exiting the LEDs were reflected or passed through a dichroic mirror (515dcxru, Chroma Technology) using an optiblock beam combiner (Prizmatix) and were focused into the epi-illumination light path of an Olympus BX51WI microscope and back aperture of a 20× water immersion objective (0.95 NA) by a dichroic mirror (700dcxxr, Chroma Technology) in the filter turret. To release glutamate from alvear terminals, three protocols were used. To assess alvear synaptic function, 10 or 20 flashes of light (0.1 ms duration at 50 ms intervals) were delivered through the objective and focused onto CA1 SO and adjacent neocortex. CA1 SR and SLM were not exposed to light. To determine alvear excitability of CA1 PCs and interneurons to theta burst stimulation, 0.1 ms flashes of blue light were delivered to the SO at 5 Hz (10 bursts separated by 200 ms intervals with each burst consisting of 5 pulses of light at 50 Hz).

Electrophysiological measurements

Whole cell patch clamp recordings from hippocampal CA1 interneurons were performed using patch pipettes (2—4 MΩ) pulled from borosilicate glass (8250 1.65/1.0 mm) on a Narishige PC-10 pipette puller filled with (in mM): $KMeSO_4$ 140, NaCl 8, MgATP 2, NaGTP 0.1, HEPES 10, and biocytin 0.1% or $CsMeSO_3$ 120, NaCl 8, MgATP 2, NaGTP 0.1, HEPES 10, $BAPTAK_4$ 10, QX 314 chloride 10, biocytin 0.1%. Membrane potentials and/or currents were measured with a Model 2400 patch clamp amplifier (A-M Systems) and converted into a digital signal by a PCI-6040E A/D board (National Instruments). WCP Strathclyde Software was used to store and analyze membrane potential and current responses on a PC computer (courtesy of Dr J Dempster, Strathclyde University). Calculated junction potentials (9.4 and 10 mV, respectively) were not compensated for in the analysis. Further analysis was performed with JuliaPro (Julia Computing), OriginPro 2018 (OriginLab Corp.) and Graphpad Prism.

Imaging of interneurons and alvear projections

Following electrophysiological recordings, slices were fixed in 4% paraformaldehyde (Boston BioProducts) and incubated

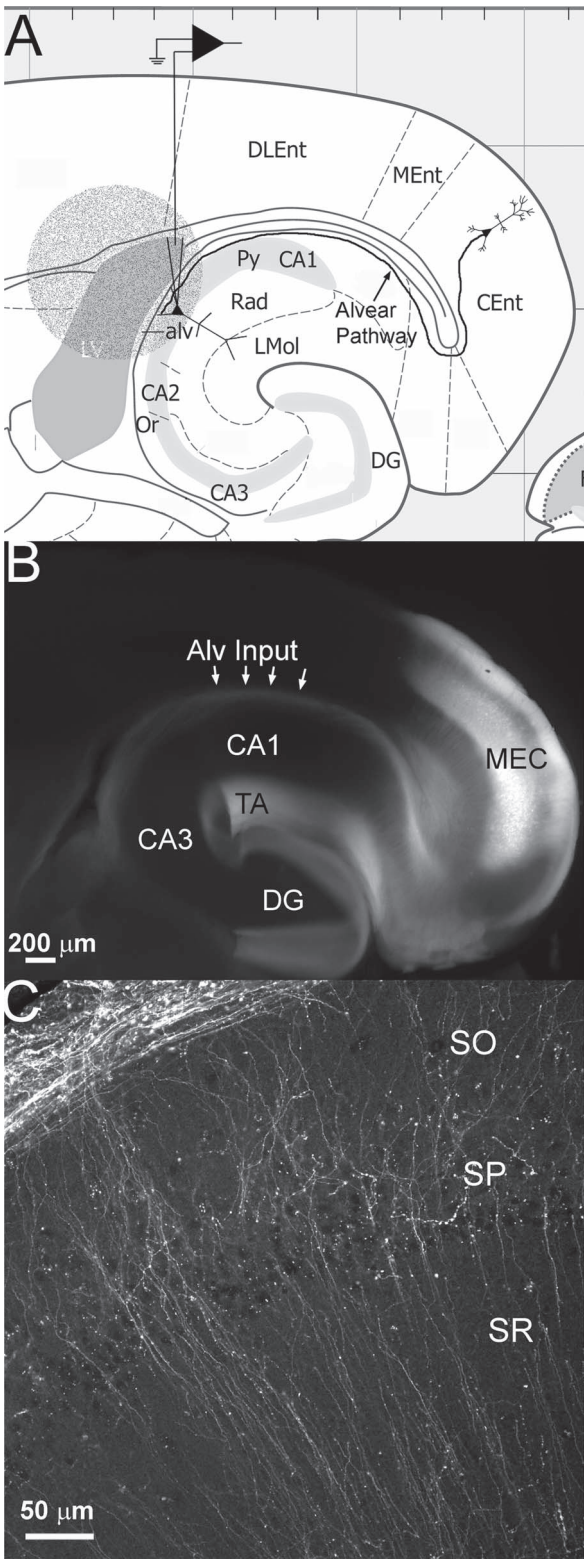

Figure 1. (*A*) Schematic of experimental set up. Horizontal section (adapted from Paxinos and Franklin 2019) illustrating the area of the horizontal brain slice illuminated for optical stimulation. The 1.1 mm diameter circle of light (round stippled area) was oriented so that the stratum pyramidale, stratum oriens, alveus and adjacent lateral ventricle and neocortex were illuminated independent of the stratum radiatum or stratum lacunosum-moleculare of hippocampal CA1. Also shown is the schematic

with streptavidin Alexa Fluor 633 (ThermoFisher Scientific) in phosphate buffered saline (PBS) with Triton-X 100 as previously described (Bell et al. 2011). Processed slices were then imaged using a Zeiss LSM 710 confocal microscope (Carl Zeiss). Alexa Fluor 633 was excited with the 633 nm line of a HeNe 5 mW laser and cells were visualized using a 20× dry lens (0.8 NA, voxel dimensions $0.2 \times 0.2 \times 1.1$ μm). Image of the oChIEF-mCitrine injection site (Fig. 1*B*) was taken with a 4× 0.16 NA Olympus objective on an Olympus BX53 microscope using a 49 020 eGFP filter cube (Chroma Technology, Bellows Falls, VT). The image was collected with an Olympus XM10 camera and stitched with cellSens software (v 1.16, Olympus). Higher magnification images of axons in the CA1c region of the hippocampus were collected with a Zeiss LSM 880 confocal microscope using a 25× 0.8 NA oil immersion objective and the 514 nm laser line.

Statistics and data analysis

Data were analyzed using WCP software and OriginPro 2018 for electrophysiological measurements. Statistics were performed using GraphPad Prism (San Diego, CA). Tests for normal distribution of data were performed using the Shapiro–Wilk test ($P < 0.05$). Data that did not pass the Shapiro–Wilk test were analyzed using the appropriate nonparametric tests indicated in the results section. Statistical significances for changes in the amplitude of excitatory postsynaptic currents (EPSCs) during stimulation trains were determined using a repeated measures one-way ANOVA with Bonferroni post hoc tests. Statistical significances of the effects of antagonists on EPSC and inhibitory postsynaptic current (IPSC) normalized amplitudes were determined by one sample *t*-tests. Comparisons between the excitability of interneuron subtypes to alvear input stimulation were assessed by two-way ANOVA with Bonferroni post hoc tests. Differences were determined to be statistically significant for *P* values less than 0.05. All data was reported as the mean, standard error of the mean (SEM). Asterisks were as follows $^{***}P < 0.001$, $^{**}P < 0.01$, $^{*}P < 0.05$.

Chemicals

All chemicals were purchased from VWR unless otherwise indicated. QX314 chloride and 4-aminopyridine (4-AP) were from Sigma-Aldrich. Tetrodotoxin citrate (TTX), bicuculline methochloride, 2,3-Dioxo-6-nitro-1,2,3,4-tetrahydrobenzo[f] quinoxaline-7-sulfonamide disodium salt (NBQX), DL-2-Amino-5-phosphono pentanoic acid (APV) were purchased from Hello Bio. Biocytin (B-1592) and streptavidin Alexa 633 were purchased from ThermoFisher Scientific.

Results

A Cre-dependent AAV containing the coding sequence for oChIEF-mCitrine was injected into the right MEC of pOXR-1-Cre mice. Four—six weeks later, the injection site in MEC as well as axons coursing in the alveus (Alv input arrows, Fig. 1*B*) and temporo-ammonic pathway (TA, Fig. 1*B*) could be observed in acute horizontal brain slices. At higher magnification, varicosities could be observed among the alvear pathway axons that travel through the alveus and adjacent CA1 SO (Fig. 1*C*). These varicosities presumably form synaptic connections with CA1 PC basal dendrites and inhibitory interneuron processes located in the deep layers of hippocampal CA1 (Deller et al. 1996). However, little is known about the physiological impact

of the alvear pathway. Therefore, we investigated the effect of alvear pathway synaptic inputs on both CA1 PCs and inhibitory interneurons in the deep layers of hippocampal CA1.

MEC alvear inputs form subthreshold facilitating excitatory synaptic connections with CA1 pyramidal neurons

We first assessed the effect of alvear pathway synaptic inputs onto CA1 PCs. To do this, we used two different transgenic mouse lines to express the optogenetic activator protein oChIEF (Lin et al. 2009) in MEC L2 and L3 projection neurons. The first transgenic line expressed Cre-recombinase under the control of the oxidation resistance protein 1 promoter, pOXR-1-Cre (Suh et al. 2011). This mouse line expresses Cre-recombinase in L3 neurons of the MEC. In this line, we intracranially injected the MEC with an adeno-associated virus (AAV) serotype 1 that expressed oChIEF-mCitrine in a Cre-dependent manner. The second transgenic mouse line expressed the tetracycline transactivator (tTA) under the control of the neuropsin promoter (NOP-tTA) (Yasuda and Mayford 2006). The NOP-tTA line expresses the tetracylcline transactivator in MEC L2 neurons as well as a smaller population of MEC L3 neurons. We expressed oChIEF-mCitrine in MEC L2 and 3 neurons by crossing the NOP-tTA line with a transgenic tTA reporter mouse line in which oChIEF-mCitrine was controlled by the tetracycline transactivator (TRE) (Cheetham et al. 2016). This cross (NOP-tTA;TRE-oChIEF-mCitrine) resulted in the expression of oChIEF-mCitrine in MEC L2 and 3 projection neurons. It should be noted that a subset of MEC L2 neurons innervate hippocampal CA1 (Kitamura et al. 2014) and thus may also contribute to the alvear pathway making both mouse models important to examine. For experiments examining alvear pathway inputs onto CA1 pyramidal neurons, we used 37 pOXR-1-Cre mice (15 male and 22 female) and 12 NOP-tTA;TRE-oChIEF-mCitrine mice (7 male and 5 female). A total of 41 of 49 pyramidal neurons responded to optogenetic stimulation of the alvear pathway. Data were pooled for analysis as two-way ANOVAs for all electrical measurements between transgenic animals and sexes were not significantly different for these and all subsequent studies. Furthermore, only preparations that demonstrated mCitrine fluorescence and had at least one neuron that responded to light stimulation were used for analysis.

We first assessed the electrophysiological properties in a subset of CA1 pyramidal neurons before examining their responses to alvear inputs (Table 2). Electrical properties of CA1 pyramidal neurons were measured from membrane potential responses to a series of current steps (600 ms) step size of 50 pA starting at −400 pA and ending at +450 pA. Action potential measurements were taken from the first action potential in the train produced by +200 pA depolarizing current pulse. The electrophysiological properties of CA1 pyramidal neurons consisted of resting membrane potential averages of -65.2 ± 0.9 mV with average action potential amplitudes of 85.8 ± 2.8 mV and durations of 1.8 ± 0.1 ms ($n = 20$). CA1 pyramidal neurons produced inwardly rectifying current–voltage relationships to hyperpolarizing current injection (Fig. 2A,D). Larger hyperpolarizing current injections produced a depolarizing sag in the membrane potential response. Suprathreshold depolarizing currents resulted in adapting trains of action potentials with small after depolarizations (Fig. 2A). Instantaneous frequencies between successive action potentials during the depolarizing pulse became smaller demonstrating spike frequency adaptation (Fig. 2B). Moreover, increasing the current pulse amplitude increased the mean action potential frequency during the depolarizing current pulse (Fig. 2C). In voltage clamp, activation of the alvear pathway with 20 Hz pulses of blue light (0.1 ms duration) resulted in facilitating EPSCs (Fig. 2G,H). EPSC amplitudes displayed a significant trend to larger successive EPSC amplitudes (Friedman test, $P < 0.0001$, $n = 7$). This suggests that the alvear pathway synaptic inputs onto CA1 pyramidal neuron basal dendrites showed a low probability of neurotransmitter release. We further determined that the synaptic delays from the light flash to the initiation of the rising phase of the EPSC was approximately 3 ms (Fig. 2I), which is consistent with a monosynaptic connection.

The activity of individual MEC L3 projection neurons in vivo has been poorly correlated with population theta rhythm activity (Quilichini et al. 2010). However, more recent studies have shown that a subset of calbindin-expressing L2 pyramidal neurons have correlated action potential activity with local population theta rhythms (Kitamura et al. 2014; Ray et al. 2014). Importantly, these calbindin-expressing L2 pyramidal neurons project to hippocampal CA1, but not DG or CA3. Furthermore, during theta rhythms the largest current sink in hippocampal CA1 occurs in the SLM and is eliminated following blockade of EC inputs (Bragin et al. 1995; Kamondi et al. 1998). Because the alvear pathway projects to hippocampal CA1 SLM, alvear inputs likely contribute to the sources and sinks observed during theta rhythm. Therefore, we examined whether theta burst activation of alvear pathway boutons in the SO of hippocampal CA1 were capable of activating CA1 pyramidal neurons. Although CA1 PCs responded by producing EPSPs, none of the 26 CA1 pyramidal neurons from which we recorded produced action potentials in response to theta burst stimulation (Fig. 2E). On average, the summating EPSPs did not exceed 3 mV in amplitude (Fig. 2F, linear trend to larger amplitudes, repeated-measures ANOVA, $P < 0.0001$, $n = 26$). Therefore, although the alvear pathway appears to innervate the basal dendrites of CA1 pyramidal neurons, synaptic release from the alvear input resulted in small subthreshold EPSPs measured at the pyramidal cell soma.

MEC alvear inputs monosynaptically excite and disynaptically inhibit CA1 pyramidal neurons

TA inputs from the MEC arise from both inhibitory and excitatory neurons (Melzer et al. 2012). However, it is unknown

of a CA1 pyramidal cell in whole cell patch clamp configuration and the alvear pathway projecting from a layer 3 neuron in the caudomedial entorhinal cortex. In other experiments, CA1 inhibitory interneurons with somas located in SO were chosen for recordings. Abbreviations: CA1, cornu ammonis 1; CA2, cornu ammonis 2; CA3, cornu ammonis 3; Cent, caudomedial entorhinal cortex; DG, dentate gyrus; DLEnt, dorsolateral entorhinal cortex; LMol, stratum lacunosum-moleculare; LV, lateral ventricle; MEnt, medial entorhinal cortex; Or, stratum oriens; Py, stratum pyramidale; Rad, stratum radiatum. Grid scale 1 mm. (*B*) Wide field fluorescent image of a 350 µm horizontal brain slice from a pOXR1-Cre mouse injected in the medial entorhinal cortex (MEC) with AAV-hSyn-Flex-oChIEF-mCitrine. Arrows point to fluorescence in the alvear pathway (Alv input). Fluorescence can also be observed in the temporo-ammonic pathway (TA). (*C*) Single plane confocal image of hippocampal CA1c next to CA2 of a pOXR1-Cre mouse injected in the MEC with AAV-hSyn-Flex-oChIEF-mCitrine. Fluorescent axons can be observed coursing through the alveus next to the stratum oriens (SO). Axons make orthogonal turns and course through the SO, SP, and SR.

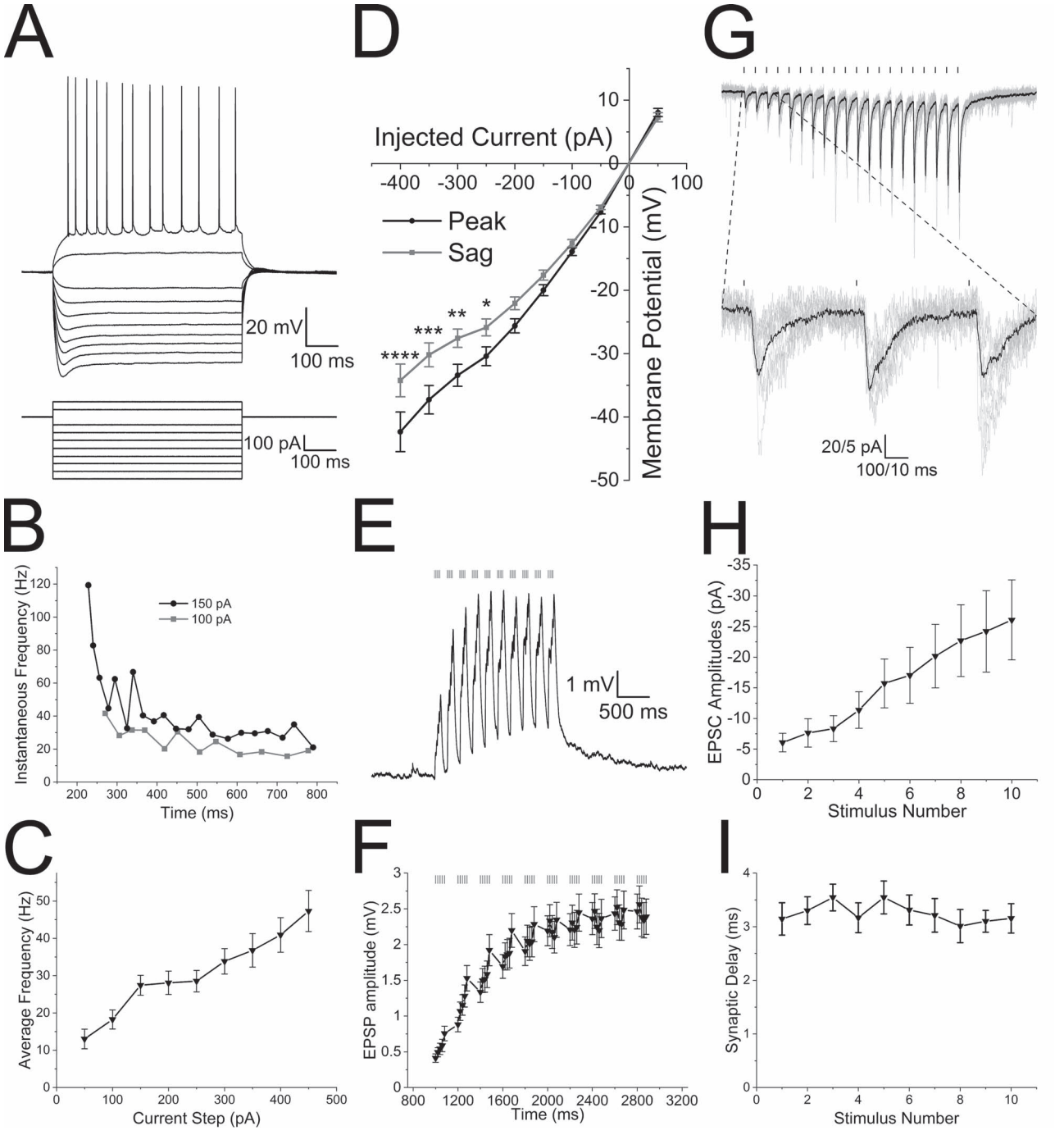

Figure 2. The alvear pathway forms functional synaptic connections onto CA1 pyramidal neurons. (*A*) CA1 pyramidal cell (PC) membrane potential responses to a series of current injections of varying amplitudes (600 ms duration). (*B*) Instantaneous frequency (Hz) of successive action potentials responding to 600 ms current pulses of varying magnitude (black 150 pA, gray 100 pA). (*C*) Average frequency of action potentials occurring during a 600 ms current pulse of varying magnitudes. (*D*) Current–voltage relationship demonstrating slight inward rectification and depolarizing sag in the membrane potential of a CA1 PC following hyperpolarizing current injections. Black line—peak voltage response amplitude, gray line—voltage response amplitude at the end of the current pulse. (*E*) Theta burst optogenetic stimulation of the alvear pathway produced subthreshold facilitating EPSPs in an individual CA1 PC (average of 10 sweeps). Bars above the voltage trace indicates the timing of blue light flashes. (*F*) Line plot of the average EPSP amplitude in response to theta burst stimulation of the alvear pathway. (*G*) Optogenetic activation of the alvear pathway produced facilitating EPSCs (20 light pulses, 0.1 ms duration, 50 ms intervals) in an individual CA1 PC. Bars above current trace indicate timing of blue light flashes. Black lines are the average of 10 trains of flashes which are superimposed by individual gray line sweeps. Below is a blow up of the first 3 blue light flashes (*H*). Line plot demonstrating that the normalized average EPSC amplitude in CA1 PCs significantly facilitated in response to 20 Hz stimulation. EPSP amplitudes significantly facilitated demonstrating a linear trend to larger amplitudes. (*I*) Synaptic delay from the blue light flash to the initiation of the rising phase of the EPSC for each of the 10 flashes during the stimuli.

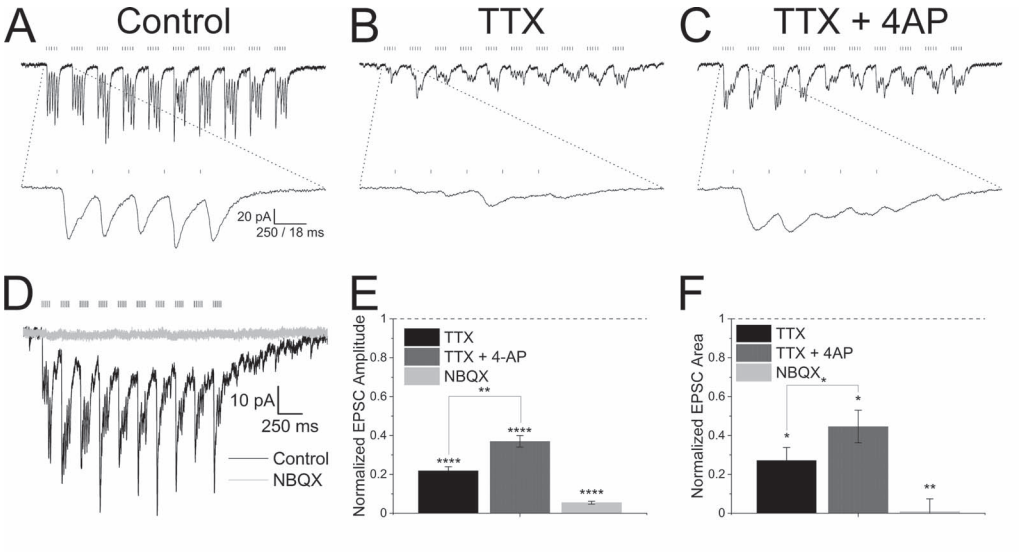

Figure 3. Alvear pathway forms monosynaptic excitatory connections onto CA1 pyramidal neurons. (*A*) Theta burst optogenetic stimulation consisting of 10 bursts of blue light pulses (5 pulses, 0.1 ms duration, 50 ms intervals) separated by 200 ms resulted in EPSCs (black trace) in a voltage-clamped PC (Vh = −65 mV). (*B*) EPSCs were partially inhibited by TTX (1 μM). (*C*) Subsequent co-application of 4-AP (100 μM) partially rescued EPSC amplitudes. (*A–C*) Bottom traces—expansion of the first optogenetic burst in the theta burst sequence. (*D*) NBQX (30 μM, gray trace) completely blocked theta burst driven EPSCs (black trace) in a CA1 pyramidal neuron (Vh = −65 mV). (*E*) Summary bar plot of the effect of TTX, TTX + 4-AP, and NBQX on the summated EPSC amplitudes. Burst amplitudes were averaged and normalized to control amplitudes. (*F*) Summary bar plot of the effect of TTX, TTX + 4-AP, and NBQX on the total EPSC burst area. Burst areas were averaged and normalized to control areas.

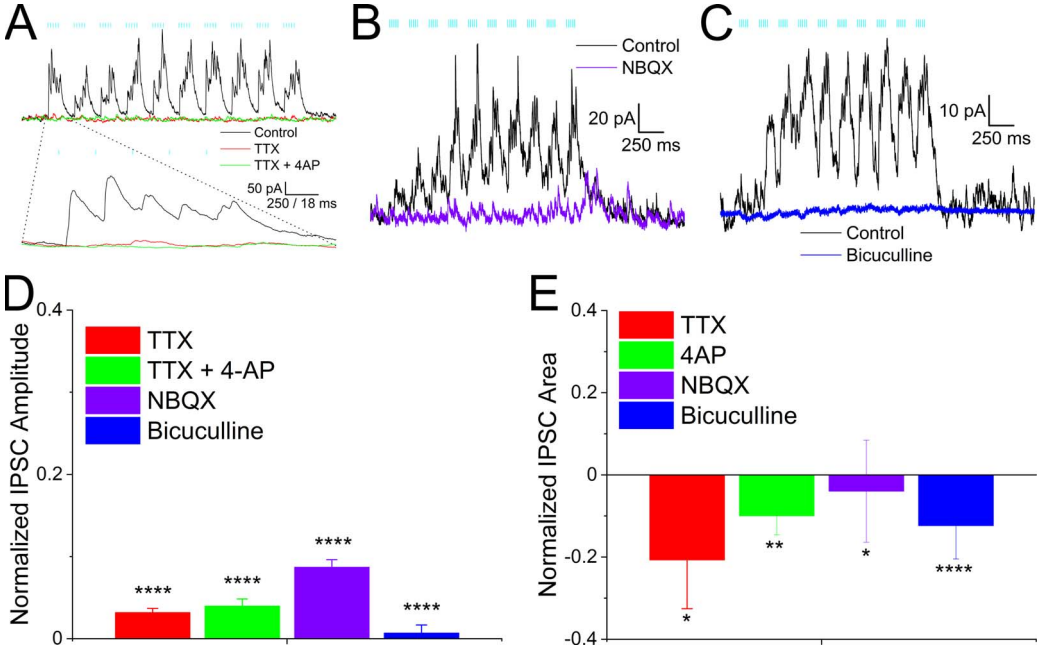

Figure 4. Alvear pathway forms disynaptic inhibitory connections onto CA1 pyramidal neurons. (*A*) Same pyramidal neuron in Figure 3 voltage clamped at +15 mV. Theta burst stimulation produced outward IPSCs (black trace) that were completely inhibited by TTX (1 μM, red trace). Subsequent addition of 4-AP (100 μM, green trace) did not rescue the TTX blockade. Bottom traces—expansion of the first optogenetic burst in the theta burst sequence. (*B*, *C*) NBQX (30 μM) completely inhibited the theta burst driven outward IPSCs in a CA1 pyramidal neuron (Vh = +15 mV). (*C*) Bicuculline (25 μM, blue trace) completely abolished the outward IPSC (black trace) in a pyramidal neuron. (*D*) Summary bar plot of the effect of TTX, TTX + 4-AP, NBQX, and bicuculline on averaged summated IPSC amplitudes. Amplitudes were normalized to control. (*E*) Summary bar plot of the effect of TTX, TTX + 4-AP, NBQX, and bicuculline on averaged total burst IPSC area. Burst areas were normalized to control.

whether alvear synaptic connections onto hippocampal neurons are excitatory or inhibitory. Therefore, we measured both EPSCs and IPSCs generated by theta burst stimulation of alvear inputs onto CA1 pyramidal neurons. For these studies we used 15 pOXR1-Cre mice (5 female, 10 male) and 14 NOP-tTA mice (4 female, 10 male). Data from all mice were pooled as no significant differences in measurements between male and female or mouse strains (two-way ANOVA).

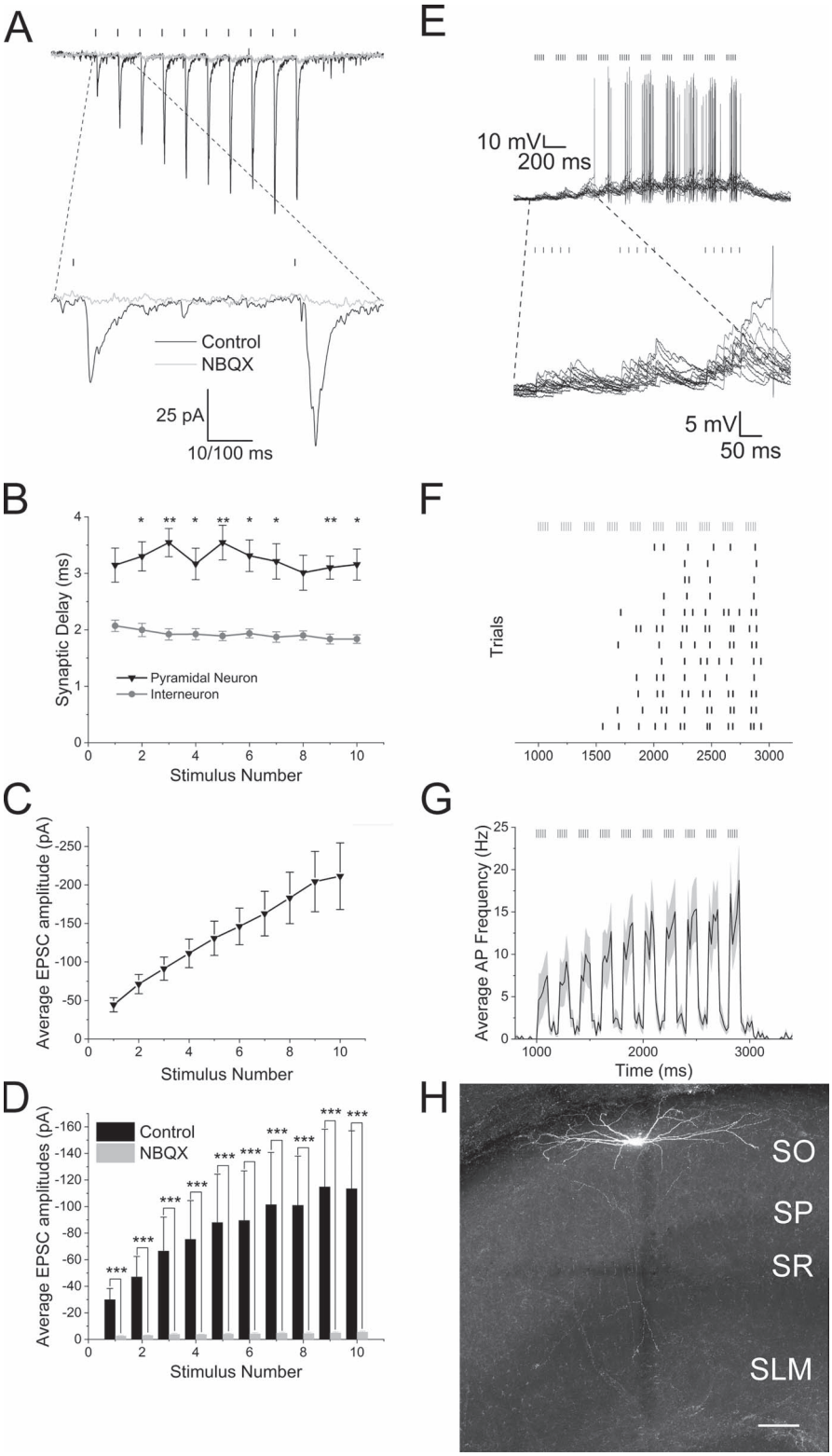

Figure 5. Alvear inputs excite CA1 inhibitory interneurons in the alveus, stratum oriens, and stratum pyramidale. (*A*) Optogenetic activation of MEC alvear inputs (10×0.1 ms blue light pulses at 20 Hz, indicated by bars above traces) produced facilitating EPSCs (black trace, average of 10 sweeps) in a CA1 stratum oriens interneuron. Application of the AMPA receptor antagonist NBQX (30 μM) inhibited the EPSCs (gray trace). (*B*) Line plot demonstrating that synaptic delays from light flash to initiation of the EPSCs were significantly faster in interneurons (gray line) versus PCs (black line). (*C*) Line plot demonstrating a consistent facilitation of alvear EPSC amplitudes (10 pulses at 20 Hz) in CA1 inhibitory interneurons. (*D*) Bar plot demonstrating that alvear EPSC amplitudes (10 pulses at 20 Hz) were reliably inhibited by the AMPA receptor antagonist NBQX. (*E*) Top: 5 Hz optogenetic theta burst stimulation of alvear inputs produced suprathreshold responses in a CA1 SO interneuron.

Optogenetic theta burst stimulation produced summating EPSCs when CA1 pyramidal neurons were voltage clamped at −65 mV, near the reversal potential for chloride (Fig. 3A). Application of the voltage-dependent sodium channel blocker, TTX, will block presynaptic action potentials and block-activity-dependent synaptic transmitter release. When we applied TTX (1 µM, Fig. 3B), EPSC amplitudes (Fig. 3E, repeated measures ANOVA, Bonferroni post hoc test, $P < 0.0001$, $n = 3$), and total area of the EPSCs (Fig. 3F, one sample t-test, $P < 0.05$) were significantly inhibited. 4-aminopyridine (4-AP), a potassium channel blocker, has been shown to rescue TTX synaptic inhibition through the inhibition of presynaptic potassium channels (Petreanu et al. 2007), presumably by permitting a larger depolarization when presynaptic terminals are optogenetically activated. When we subsequently applied 4-AP (100 µM) after TTX inhibition, EPSCs were moderately rescued particularly during the initial stimuli in a burst (Fig. 3E, repeated measures ANOVA, Bonferroni post hoc test, $P = 0.0019$, $n = 3$, EPSC normalized amplitudes from the 7th stimulus in 4-AP did not pass the Shapiro–Wilk test for normality). Similarly, total area of the EPSC burst displayed significant recovery from TTX inhibition following the application of 4-AP (paired t-test, $P < 0.05$, $n = 3$). These observations suggest that the EPSCs in CA1 pyramidal neurons resulted from monosynaptic inputs from the MEC alvear pathway (Petreanu et al. 2007). Furthermore, these observations suggest that the synaptic connections were local to the light stimulus in the SO and not due to the propagation of action potentials to the SLM.

We next examined the receptor subtypes mediating postsynaptic responses in CA1 PCs. Application of the AMPA receptor antagonist NBQX (30 µM) completely inhibited EPSC amplitudes (Fig. 3D,E, one sample t-test, $P < 0.0001$, $n = 3$) and EPSC total burst area (Fig. 3F, one sample t-test, $P < 0.01$, $n = 3$). This suggests that alvear inputs release glutamate to mediate their effect.

To record inhibition produced by MEC alvear stimulation, the membrane potential was held at approximately +15 mV near the reversal potential for ionotropic glutamate receptors. Optogenetic theta burst stimulation at +15 mV resulted in outward IPSCs (Fig. 4A, black trace) that were completely blocked by TTX (1 µM, Fig. 4A,D, red, repeated-measures ANOVA, $P < 0.0001$, Bonferroni post hoc test, $P < 0.0001$, $n = 3$). However, unlike alvear EPSCs, the IPSCs were not rescued by subsequent addition of 4-AP (100 µM, Fig. 4A,D, Bonferroni post hoc test, $P = 0.8$, $n = 3$, EPSP normalized amplitudes from the 10th stimulus in 4-AP did not pass the Shapiro–Wilk test for normality). We also measured the total area mediated by the burst IPSCs (Fig. 4E). Similar to the amplitude measurement, IPSC area was significantly inhibited by TTX (one sample t-test, $P < 0.05$, $n = 3$), but application of 4-AP did not recover the inhibition mediated by TTX (paired t-test, $P = 0.35$). These data suggest that the MEC alvear pathway can inhibit CA1 pyramidal neurons indirectly through the excitation of inhibitory interneurons.

We next examined which receptor subtypes mediated the alvear driven IPSCs in CA1 pyramidal cells. Because MEC inputs were thought to be mediated by glutamate release, we first tested whether IPSCs could be inhibited by the glutamate receptor antagonist NBQX. NBQX (30 µM) completely antagonized the outward currents (Fig. 4B purple). The inhibition of the IPSCs by NBQX was observed in both amplitude (Fig. 4D purple, one sample t-test, $P < 0.0001$, $n = 3$) and total burst IPSC area measurements (Fig. 4E purple, one sample t-test, $P < 0.05$, $n = 3$). These data suggested that the alvear pathway elicited feedforward inhibition of CA1 pyramidal neurons through the activation of inhibitory interneurons. We next tested which inhibitory receptors mediated the multi-synaptic IPSCs. Application of the $GABA_A$ receptor antagonist bicuculline at 25 µM completely inhibited the outward currents (Fig. 4C, blue trace). Both the amplitudes (Fig. 4D blue, one sample t-test, $P < 0.0001$, $n = 10$) and the total IPSC burst area (Fig. 4E blue, one sample t-test, $P < 0.0001$, $n = 10$) were significantly blocked by bicuculline. Therefore, these data suggest that glutamatergic inputs mediated both the monosynaptic excitatory inputs and the indirect activation of inhibitory inputs onto CA1 PCs by the alvear pathway. Interneurons excited by alvear inputs then inhibit postsynaptic CA1 PCs via the activation of $GABA_A$ receptors.

MEC alvear inputs excite horizontally-oriented interneurons in stratum oriens of hippocampal CA1

Although activation of alvear inputs does not appear to be potent enough to elicit action potentials in CA1 PCs, the same activation does elicit inhibitory synaptic responses in CA1 PCs (Fig. 4). Therefore, we next examined the effect of optogenetic stimulation of alvear inputs on inhibitory interneuron activity in hippocampal CA1. In total, we recorded from 39 interneurons with somas located in hippocampal CA1 SO. We included biocytin in the patch pipette to aid in the identification of these interneurons. Out of 39 interneurons, 11 did not respond. Of the remaining 28 interneurons, 15 could not be reconstructed, and the remaining 13 had soma and dendrites confined to the SO (e.g., Fig. 5H) demonstrating that these interneurons could only be activated by axon terminals in the SO and not the SLM. However, none of these 13 neurons had sufficient axonal fill to permit anatomical identification.

We first examined the strength of alvear inputs by optogenetically stimulating their afferents (10 blue light pulses, 0.1 ms duration, 50 ms intervals) and assessing short-term synaptic dynamics. All interneurons responded with facilitating EPSCs (Fig. 5A, black trace). Synaptic delays from the light pulse to the initiation of the rising phase of the EPSC were approximately 2 ms, significantly shorter than the synaptic delays onto CA1 pyramidal neurons (Fig. 5B, two-way ANOVA, $P < 0.0001$). The EPSC facilitation showed a significant linear trend to larger amplitudes with subsequent stimuli (Fig. 5C, repeated-measures ANOVA, linear trend, $P < 0.0001$, $n = 10$). EPSCs in all interneurons were blocked by the glutamatergic AMPA receptor antagonist NBQX at 30 µM (Fig. 5A,D gray trace/bar, two-way ANOVA, Bonferroni post hoc test, $P < 0.0001$, $n = 10$). Therefore, the alvear inputs appear to have a low probability of release, have synaptic delays consistent with monosynaptic activation, and were mediated by

Bars above 10 superimposed traces indicate timing of light flashes. Bottom: Blow up of the first 3 theta bursts. (F) Raster plot of the timing of action potentials that occurred during each trial taken from the sweeps of E. (G) Peristimulus time histogram of the mean action potential firing frequency (20 ms bins) averaged from 22 different CA1 alvear/stratum oriens/stratum pyramidale interneurons in response to 5 Hz optogenetic stimulation of the alvear pathway. Gray shading indicates the SEM. (H) Confocal image of a horizontal CA1 inhibitory interneuron that was excited by optogenetic activation of alvear inputs and has its soma and dendrites confined to the SO. Scale—100 µm.

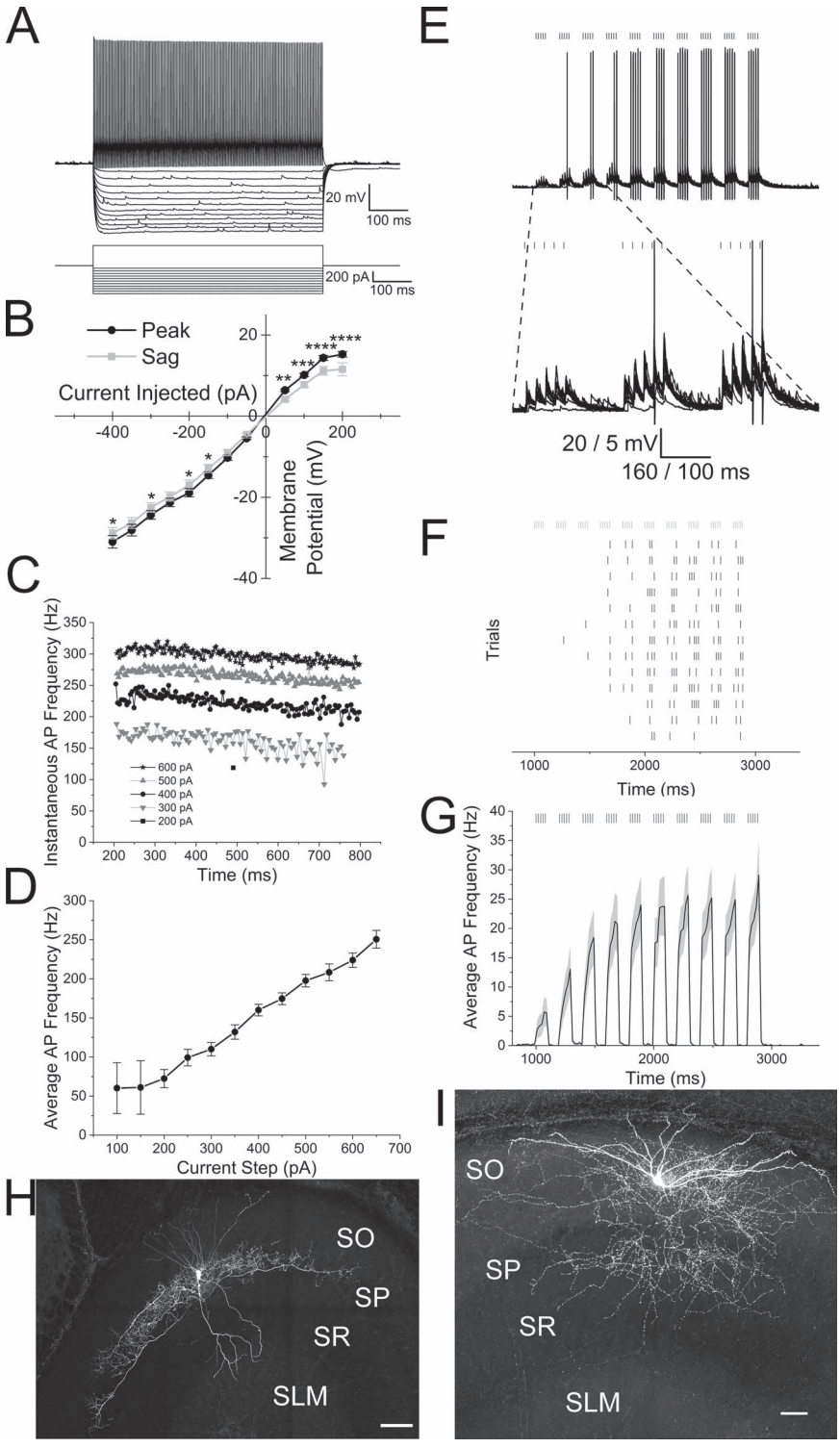

Figure 6. Alvear inputs excite hippocampal CA1 parvalbumin-expressing interneurons. (*Ai*) Membrane potential responses of a PV interneuron (top) to steps of current injection (bottom). (*B*) Line plot illustrating the membrane potential amplitude responses to current injections (black line—maximum voltage response (peak), gray line—membrane potential amplitude at end of response (sag)). (*C*) Line plot of the instantaneous frequencies between successive action potentials during a 600 ms depolarizing step. Different step magnitudes are indicated in legend. (*D*) Line plot of the average action potential frequency during a 600 ms depolarizing step plotted against current step magnitudes. (*E*) Top. Theta burst optogenetic stimulation of MEC alvear inputs evoked rhythmic action potential firing in a PV interneuron (13 overlapping sweeps). Bottom. Blow up of the first three optogenetic bursts (action potentials truncated). Black lines over traces indicated timing of light flash. (*F*) Raster plot of the timing of each action potential during individual sweeps. Gray lines over traces indicated timing of light flash. (*G*) Peristimulus time histogram of the mean action potential firing frequency (20 ms bins) averaged from 29 PV interneurons that responded with action potentials to alvear pathway optogenetic theta burst stimulation. Gray shading indicates SEM. (*H*) Confocal image of a PV interneuron with perisomatic axonal arborization that responded to alvear stimulation. (*I*) Confocal image of a PV interneuron with bistratified axonal arborization that responded to alvear stimulation. Scale bars: H-50 µm and I-100 µm.

Table 2 Electrophysiological properties of known cell types from which recordings were made in this study

Cell type	AP Amplitude (mV)	AP threshold (mV)	AP duration (ms)	AP mean frequency (Hz)	AP adaptation frequency ratio (first/last)	Resting Membrane Potential (mV)	Input Resistance (mΩ)	Membrane Time Constant (ms)	Cell Capacitance (pF)	I_h Sag Ratio
CA1 Pyramidal Cell ($n = 20$)	85.8 ± 2.8	−43.9 ± 0.8	1.77 ± 0.11	35.9 ± 3.0	0.36 ± 0.04	−65.2 ± 0.9	180.7 ± 18.7	17.0 ± 1.2	110.9 ± 13.5	0.82 ± 0.01
PV Interneuron ($n = 58$)	69.0 ± 1.5	−42.8 ± 0.9	0.51 ± 0.01	184.8 ± 7.1	1.30 ± 0.23	−61.6 ± 0.9	111.0 ± 7.6	7.5 ± 0.5	73.1 ± 4.5	0.93 ± 0.005
VIP Interneuron ($n = 16$)	74.3 ± 2.4	−40.8 ± 0.8	1.01 ± 0.03	64.1 ± 8.5	0.42 ± 0.04	−59.3 ± 1.0	492.7 ± 58.6	28.5 ± 4.7	58.1 ± 4.1	0.84 ± 0.02
GIN Interneuron ($n = 29$)	64.0 ± 2.5	−38.4 ± 1.2	0.90 ± 0.04	65.2 ± 4.8	0.74 ± 0.09	−57.0 ± 1.3	394.7 ± 42.0	35.6 ± 3.1	110.7 ± 9.0	0.84 ± 0.02

glutamatergic receptors on horizontally oriented interneurons in hippocampal CA1.

We next examined the excitability of CA1 SO neurons to 5 Hz theta burst optogenetic stimulation. Of the 28 interneurons that responded to alvear stimulation, 17 interneurons fired action potentials during theta burst stimulation (Fig. 5E–G). Of those 17 activated interneurons, seven had sufficient biocytin reconstruction to show soma and dendrites confined to stratum oriens with two having axonal fills consistent with perisomatic interneurons and one with bistratified-like axonal arborization. Averaging the peristimulus time histogram data among all responding SO interneurons demonstrated that the average frequency of action potentials increased with subsequent optogenetic bursts (Fig. 5G). Therefore, these data demonstrated that alvear inputs could excite inhibitory interneurons in hippocampal CA1 and produce feedforward inhibition of CA1 pyramidal neurons.

Parvalbumin-expressing hippocampal CA1 interneurons can be activated by alvear inputs

TA inputs from the entorhinal cortex innervate hippocampal CA1 in the SLM. Stimulation of the TA has been shown to activate interneurons that in turn activate both $GABA_A$ and $GABA_B$ receptors on CA1 PCs (Empson and Heinemann 1995a, 1995b; Dvorak-Carbone and Schuman 1999; McQuiston 2011; Milstein et al. 2015). However, stimulation of axons in the SLM failed to activate parvalbumin-expressing (PV) interneurons (Milstein et al. 2015). These latter studies suggest that the entorhinal cortex may play a limited role in inhibiting CA1 PC output and may not contribute to behaviorally-relevant rhythmicity as PV interneurons play major roles in both these processes (Pelkey et al. 2017). However, alvear pathway terminals in CA1 are located in a position where they could activate PV interneurons. The next set of experiments examined whether PV interneurons in CA1 responded to alvear pathway stimulation.

To target PV interneurons, we crossed NOP-tTA;oChIEF-mCitrine or pOXR-1-Cre mice to transgenic mice expressing tdTomato under the control of the parvalbumin promoter (Kaiser et al. 2016) or homozygous crosses of PV-Cre (Hippenmeyer et al. 2005) and Ai14 (Madisen et al. 2010). Recordings from tdTomato-positive (PV) interneurons displayed fast action potentials with little adaptation when depolarized by current injection (Fig. 6A,C). Increasing current step amplitudes increased the average action potential frequency (Fig. 6D). These interneurons also produced slightly inwardly rectifying hyperpolarizations with a small amount of depolarizing sag in response to hyperpolarizing current injection (Fig. 6A,B, two-way ANOVA, $P < 0.0001$). The electrophysiological properties of these interneurons consisted of resting membrane potential averages of -61.2 ± 0.8 mV, input resistances of 111.0 ± 7.7 MΩ, 69.0 ± 1.5 mV action potential amplitudes and 0.51 ± 0.01 ms action potential durations (Table 2, $n = 58$). Post hoc anatomical reconstruction of biocytin-filled PV interneurons showed that 29 cells had perisomatic axonal arborizations (Fig. 6H), five had bistratified morphology (Fig. 6I) and 24 did not have sufficient axonal fill to determine anatomical subtype.

We next examined whether action potentials could be produced in PV interneurons by optogenetic theta burst activation of alvear pathway inputs. 5 Hz optogenetic theta burst stimulation of the alvear pathway resulted in the production of action potentials in 29 interneurons. Of the interneurons that produced suprathreshold responses, 18 were perisomatic (Fig. 6H), one

was bistratified (Fig. 6I), and 10 had insufficient biocytin fills for anatomical identification. Of the 18 perisomatic interneurons that responded with action potentials to theta burst stimulation, 13 were horizontal and 5 had vertically oriented dendrites. In each responsive interneuron, 5 Hz optogenetic theta burst stimulation reliably produced action potentials during each trial (Fig. 6E,F). When all action potential responsive interneurons were averaged and peristimulus time histograms constructed, 5 Hz optogenetic theta burst stimulation resulted in peak burst frequencies near 25 Hz (Fig. 6G). Therefore, unlike the perforant path (Milstein et al. 2015), 5 Hz theta burst activation of the entorhinal cortical alvear pathway was capable of activating both perisomatic and bistratified PV interneurons in hippocampal CA1.

VIP-expressing CA1 hippocampal interneurons can be activated by alvear inputs

In addition to PV-expressing neurons, a subset of VIP-expressing interneurons constitute another class of perisomatic projecting interneurons onto CA1 PCs (Klausberger and Somogyi 2008; Pelkey et al. 2017). In order to target VIP-expressing cells for the next set of experiments, we crossed either NOP-tTA;oChIEF-mCitrine or pOXR-1-Cre mice with homozygous crosses of a VIP-Cre driver mouse line (Taniguchi et al. 2011) and a tdTomato Cre-dependent reporter mouse line (VIP-Cre;ai14) (Madisen et al. 2010). pOXR-1-Cre;VIP-Cre;ai14 crosses were injected with AAV-hSyn-Flex-oChIEFmCitrine into the MEC. tdTomato-expressing VIP interneurons were targeted for whole cell patch clamp recordings, and electrophysiological responses to optogenetic stimulation were measured from recorded neurons.

VIP-expressing interneurons had varying electrophysiological properties. Perisomatic VIP-expressing interneurons had regular spiking firing patterns with adapting action potential frequencies (Fig. 7A,C; Bell et al. 2015). Increasing current injection amplitudes increased the average frequency of action potentials that occurred during the current step (Fig. 7D). Current voltage relationships showed slight inward rectification with a small depolarizing sag in the membrane response to hyperpolarizing currents (Fig. 7B, two-way ANOVA, $P < 0.0001$, $n = 11$). Averaged electrophysiological properties of these interneurons were defined by -59.3 ± 0.1 mV resting membrane potentials, 492.7 ± 58.6 MΩ input resistances, 74.3 ± 2.4 mV action potential amplitudes, and 1.01 ± 0.03 ms action potential durations. When we delivered optogenetic theta burst stimulation to 37 VIP-expressing interneurons, 16 VIP interneurons responded by producing action potentials, (Fig. 7E,F), 12 responded with subthreshold excitatory postsynaptic potentials, and nine displayed no response. Of the 16 interneurons that produced action potentials, four had perisomatic axonal arborizations, three had non-perisomatic morphology, and nine could not be identified. Of the 10 interneurons that responded with subthreshold EPSPs, two had perisomatic axonal arborizations whereas the other 10 could not be anatomically identified.

An example of a VIP interneuron that responded to 5 Hz optogenetic theta burst stimulation is illustrated in Figure 7E. Theta burst optogenetic stimulation resulted in burst firing synchronized to the optogenetic stimulation (Fig. 7E,F). When the action potential frequency of the 16 responding interneurons were averaged, the first 2 optogenetic bursts produced low frequencies of action potentials. The average frequency of action potentials during bursts continued to increase with subsequent optogenetic bursts peaking near 13 Hz (Fig. 7G, Civ). Therefore, like PV-expressing interneurons, VIP interneurons were excited with theta burst optogenetic stimulation of alvear inputs; however, these interneurons responded with lower frequency of action potentials.

A small population of presumptive oriens lacunosum-moleculare interneurons are activated by alvear inputs

We next examined the effect of optogenetic activation of the alvear pathway on the excitability of a subpopulation of OL-M interneurons in hippocampal CA1, which innervate the distal apical dendritic domain of CA1 PCs. Transgenic GFP interneuron mice (GIN mice) used in these studies express GFP in a subpopulation of somatostatin interneurons with axon arborizations in the stratum lacunosum-moleculare in hippocampal CA1 and CA3 (Oliva Jr. et al. 2000). We crossed these GIN mice with either NOP-tTA;oChIEF-mCitrine or pOXR-1-Cre mice to target OL-M cells. The alvear pathway was optogenetically stimulated to assess responses in GIN cells.

The electrical properties of GIN interneurons in hippocampal slices had regular or burst spiking with adapting action potential firing patterns when depolarized by positive current steps (Fig. 8A,C). Increasing the current step amplitude increased the average frequency of action potentials (Fig. 8D). When these interneurons were hyperpolarized by negative current steps, the cell responded with inward rectification and a depolarizing sag in the hyperpolarizing membrane potential response (Fig. 8B, two-way ANOVA, $P < 0.0001$, $n = 11$). The electrophysiological properties of these interneurons consisted of resting membrane potential averages of -57.0 ± 1.3 mV, input resistances of 394.7 ± 42.0 MΩ, 64.0 ± 2.5 mV action potential amplitudes and 0.90 ± 0.04 ms action potential durations. Optogenetic theta burst stimulation of the alvear pathway induced a small subpopulation of these interneurons to fire action potentials. The GIN interneuron illustrated in Figure 8E responded with action potentials to 5 Hz optogenetic theta burst stimulation. During each trial, this cell produced action potentials sporadically with less than 10 action potentials per sweep (Fig. 8F). For seven interneurons that responded with action potentials to 5 Hz optogenetic theta burst stimulation, the average action potential frequencies were below 15 Hz (Fig. 8G). Although we attempted to morphologically identify the GIN interneurons following our recordings, none of the biocytin fills provided enough axon arborization for interneuron subtype identification (Fig. 8H). Therefore, although some GIN interneurons could be excited by optogenetic theta burst stimulation, they typically responded sporadically with low frequencies of action potentials.

In summary, the responsiveness of PV, VIP, and GIN interneurons to alvear pathway stimulation varied across subtypes. GIN neurons showed considerably less responsiveness to alvear input. Specifically, 85% of GIN neurons did not respond to alvear stimulation compared to 25% of PV and 30% of VIP interneurons that were non responsive (Fig. 9B). Of the interneurons that fired action potentials, PV interneurons produced a significantly higher frequency of action potentials during each burst of a 5 Hz optogenetic theta burst stimulation (Fig. 9A, Friedman test, $P < 0.0001$, Dunn's multiple comparisons test, $P < 0.0001$: PV vs. VIP, $P < 0.05$: PV vs. GIN). Therefore, PV interneurons appear to be more excitable to MEC alvear inputs compared to interneurons that express VIP or somatostatin.

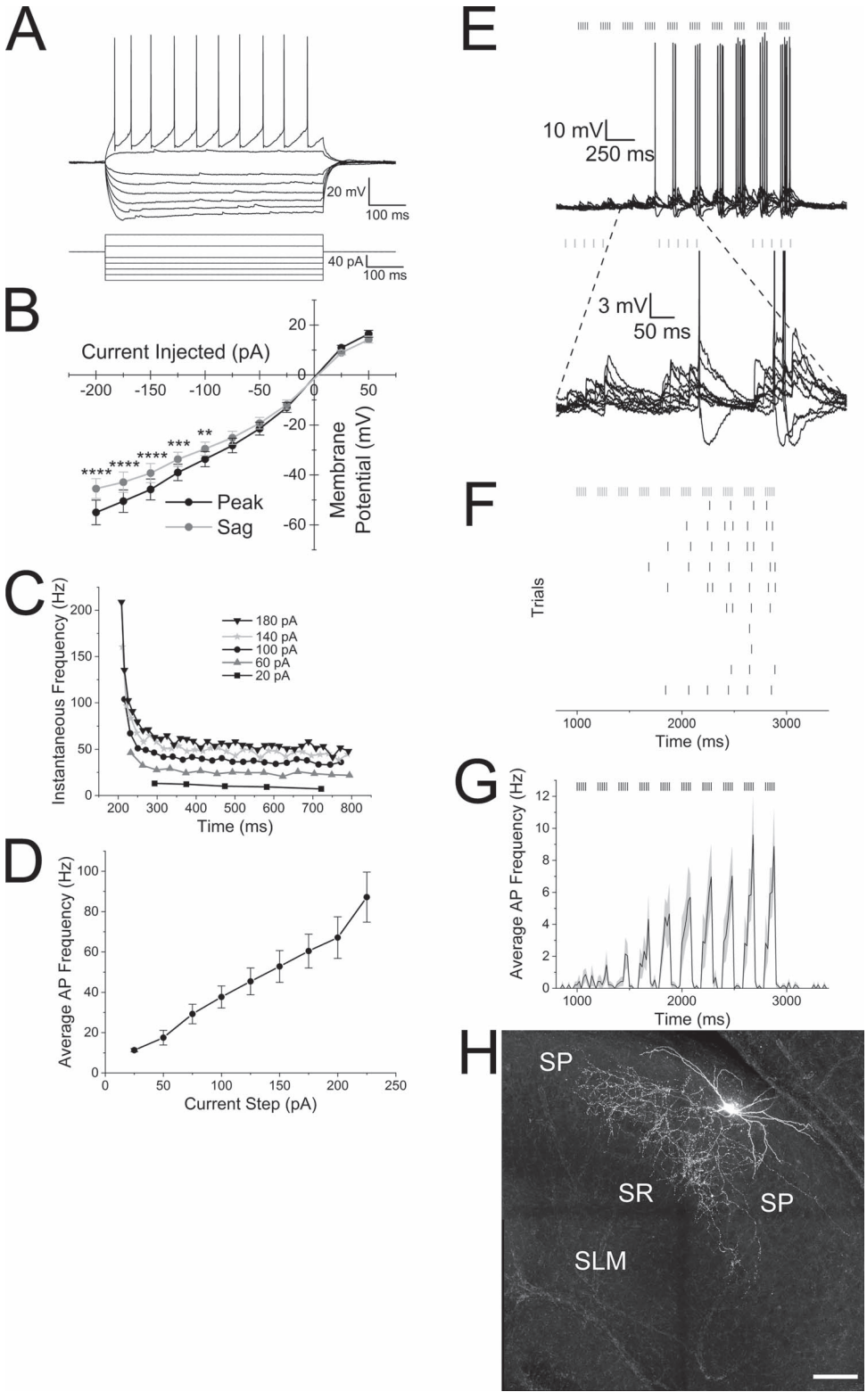

Figure 7. Alvear inputs excite VIP-expressing interneurons in stratum oriens of hippocampal CA1. (*A*) Membrane potential response of a VIP interneuron to depolarizing and hyperpolarizing current injections. (*B*) Line plot illustrating the membrane potential amplitude responses to current injections (black line—maximum voltage response [peak], gray line—membrane potential amplitude at end of response [sag]). (*C*) Line plot of the instantaneous frequency between successive action potentials during 600 ms depolarizing current pulses. Current step magnitudes indicated in the legend. (*D*) Line plot of the average action potential frequency of VIP interneurons during different depolarizing current steps. (*E*) Top: 10 superimposed membrane potential traces of a VIP interneuron in response to 5 Hz optogenetic theta burst

Suppression of PV interneuron activity inhibits alvear-driven inhibitory postsynaptic currents in hippocampal CA1 pyramidal neurons

Hippocampal CA1 PV interneurons appear to be largely unaffected by TA inputs located in the SLM of CA1 (Milstein et al. 2015). However, both perisomatic and bistratified PV interneurons located in deep layers of hippocampal CA1 can be excited to produce action potentials by stimulation of the alvear pathway (Fig. 6). Therefore, we examined the contribution of PV interneurons to the multi-synaptic IPSCs measured in hippocampal CA1 pyramidal neurons during theta burst stimulation of alvear inputs.

To do this we crossed NOP-tTA;oChIEF-mCitrine mice with mice that expressed the inhibitory optogenetic protein Arch-GFP in PV interneurons (PV-Cre;Ai35) (Hippenmeyer et al. 2005; Madisen et al. 2010). In all crosses, alvear terminals were excited with 5 Hz optogenetic theta burst stimulation either with or without a concurrent orange light flash to silence PV interneurons (3000 ms duration) (Fig. 10). In mice without Arch-GFP containing PV cells, orange light had no effect on the IPSC amplitudes (Fig. 10C,D, $n = 6$). In contrast, orange light could completely suppress theta burst generated IPSCs in mice expressing Arch (Fig. 10A,B, $n = 6$). When we examined normalized IPSC amplitudes, orange light significantly suppressed IPSC amplitudes in mice that expressed Arch in PV interneurons (Fig. 10E, $P < 0.0001$ two-way ANOVA, Bonferroni post hoc test, IPSC 1st burst amplitude distribution in Arch containing slices did not pass the Shapiro–Wilk normality test). The average magnitude of the orange light suppression in Arch-GFP PV interneurons was greater than 50% (orange light = 41.2 ± 3.8% control amplitudes). Similarly, Arch-GFP activation significantly reduced the total IPSC area (Fig. 10F,G, paired t-test, $P < 0.01$, $n = 6$). Therefore, these interneurons contributed significantly to alvear pathway feedforward inhibition of CA1 pyramidal neurons in our mouse models.

Discussion

Our results suggest that alvear inputs from the MEC were capable of producing facilitating low probability release glutamatergic synapses onto both PCs and interneurons in the SO of hippocampal CA1. The alvear inputs onto the basal dendrites of CA1 PCs produced subthreshold EPSPs even under robust theta burst stimulation paradigms. In contrast, theta burst stimulation of alvear inputs strongly activated horizontally oriented interneurons in the SO of CA1 producing suprathreshold responses. However, not all interneuron subtypes were equally affected by alvear inputs. PV perisomatic interneurons responded more robustly to alvear theta burst stimulation by producing higher frequencies of action potentials compared to VIP and GIN interneurons. Furthermore, optogenetic silencing of PV interneurons during alvear theta burst stimulation suppressed disynaptic rhythmic IPSCs in CA1 PCs by greater than 50%. Therefore, MEC alvear inputs appeared to primarily influence hippocampal CA1 via feedforward inhibition. This pathway may contribute to the generation of rhythmic perisomatic inhibition observed during theta rhythms in hippocampal CA1 PCs (Soltesz and Deschenes 1993).

In contrast to the alvear pathway, the EC TA pathway synapses on the distal apical dendrites of CA1 PCs in the SLM (Steward 1976; Steward and Scoville 1976). There is some disagreement on whether stimulation of the EC in vivo is capable of eliciting suprathreshold excitation of CA1 PCs (Andersen et al. 1966; Segal 1972; Yeckel and Berger 1990; Leung et al. 1995; Yeckel and Berger 1995). However, ex vivo stimulation of the TA or direct activation of the SLM has consistently been found to result in subthreshold EPSPs in CA1 PCs (Colbert and Levy 1992; Empson and Heinemann 1995a, 1995b; Ang et al. 2005). Furthermore, in the absence of synaptic inhibition, stimulation of the SLM produced facilitating EPSPs suggestive of a low probability release synapse (McQuiston 2007, 2008). Thus, MEC alvear terminals appear to be similar TA terminals and resulted in facilitating EPSCs indicative of a low probability release synapse.

MEC alvear inputs onto CA1 PCs also appear to be monosynaptic because TTX did not completely eliminate EPSCs in CA1 PCs, and the potassium channel blocker 4-AP partially rescued the response to alvear input. Furthermore, because the light stimulus was confined to the SP and SO, axon terminals in these layers must be the source of the EPSCs and not the result of the propagation of action potentials to terminals in the SLM. Synaptic delays of alvear inputs were approximately 3 ms for PCs further supporting monosynaptic nature of alvear inputs onto PC basal dendrites in the deep layers of hippocampal CA1. Furthermore, MEC alvear excitatory inputs onto CA1 PCs were mediated by glutamate receptor activation.

In contrast, TTX completely inhibited MEC alvear input mediated IPSCs in CA1 PCs. Importantly, 4-AP could not rescue the IPSCs inhibited by TTX in CA1 PCs. These results suggest that inhibitory synaptic transmission driven by MEC alvear input stimulation was not monosynaptic. Furthermore, the IPSCs in CA1 PCs were blocked by both AMPA receptor antagonists and $GABA_A$ receptor antagonists. These findings suggest that MEC alvear inputs drive disynaptic inhibition in hippocampal CA1 PCs. Therefore, although alvear inputs monosynaptically excite CA1 PCs, the predominant effect of MEC alvear inputs on CA1 PC activity may be through disynaptic inhibition.

Consistent with alvear disynaptic inhibition of CA1 PCs, activation of MEC alvear inputs produced EPSCs in CA1 interneurons. These EPSCs were facilitating, suggesting that MEC alvear inputs onto interneurons had a low probability of release. The synaptic delay of alvear inputs onto CA1 interneurons was approximately 2 ms, which was significantly shorter than the delay onto CA1 PCs. This suggests that alvear inputs onto CA1 interneurons are also monosynaptic. Furthermore, the MEC alvear inputs were also mediated by glutamate receptors. Post hoc anatomical reconstruction of these CA1 SO interneurons showed that they had horizontal somatodendritic morphology, some of which had axons confined to the PC cell body layer. Given that these interneurons were confined to SO, alvear pathway activation must arise from activation of postsynaptic

stimulation. Bars above the traces indicate the timing of the blue light pulses. Bottom: Blow up of bursts 2—4. (*F*) Raster plot of the timing of action potentials occurring during each of the 10 individual trials of the interneuron shown in *E*. (*G*) Averaged peristimulus time histogram of the mean action potential firing frequency (20 ms bins) taken from 14 VIP interneurons that produced action potentials to 5 Hz optogenetic theta burst stimulation. Gray shading indicates the SEM. (*H*) Confocal image of a VIP perisomatic interneuron that responded to alvear input stimulation. Scale bar—100 µm.

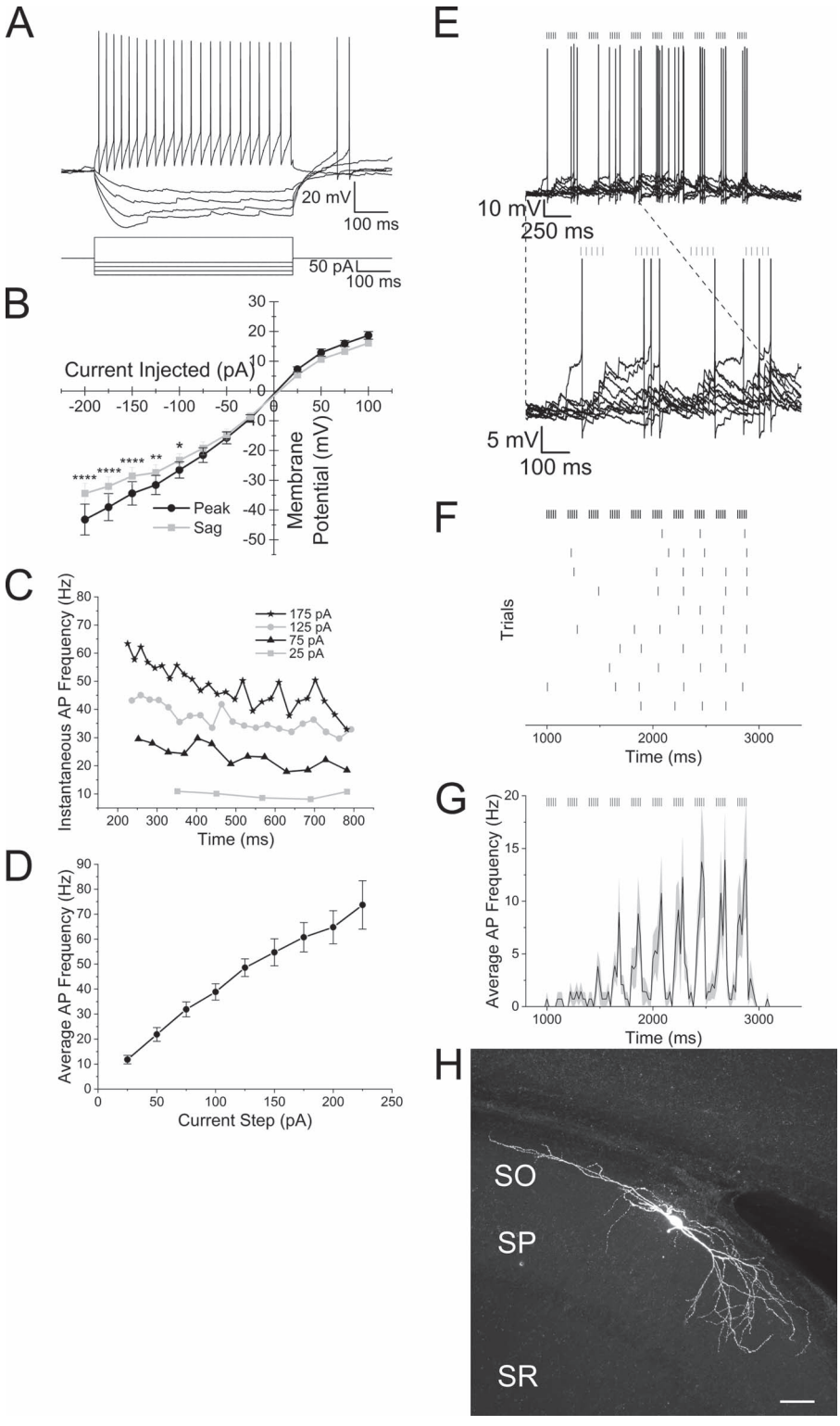

Figure 8. A small subset of oriens lacunosum-moleculare interneurons in hippocampal CA1 are activated by alvear inputs from the entorhinal cortex. (*A*) Membrane potential responses of a GIN interneuron to depolarizing and hyperpolarizing current responses. (*B*) Line plot illustrating membrane potential amplitude responses to a series of current injection steps (black line—maximum voltage response [peak], gray line—membrane potential amplitude at end of response [sag]). (*C*) Line plot of the instantaneous frequency of successive action potentials produced by different depolarizing current injections. Legend shows current pulse magnitudes. (*D*) Line plot of the average action potential frequency during depolarizing current injections of varying magnitude. (*E*) Top: 10 superimposed traces of the response of a GIN interneuron to 5 Hz optogenetic theta burst stimulation of the alvear pathway. Vertical lines above the traces indicate the timing of the blue light flashes. Bottom: Blowup of the first 4 bursts. (*F*) Raster plot of the timing of action potentials in the GIN interneuron shown in *E* to 5 Hz optogenetic theta burst stimulation of the alvear pathway. (*G*) Average peristimulus time histogram (20 ms bins) taken from 7 GIN neurons that responded with action potentials to 5 Hz optogenetic theta burst stimulation. (*H*) Confocal image of GIN neuron that responded to blue light pulses. Scale bar—50 µm.

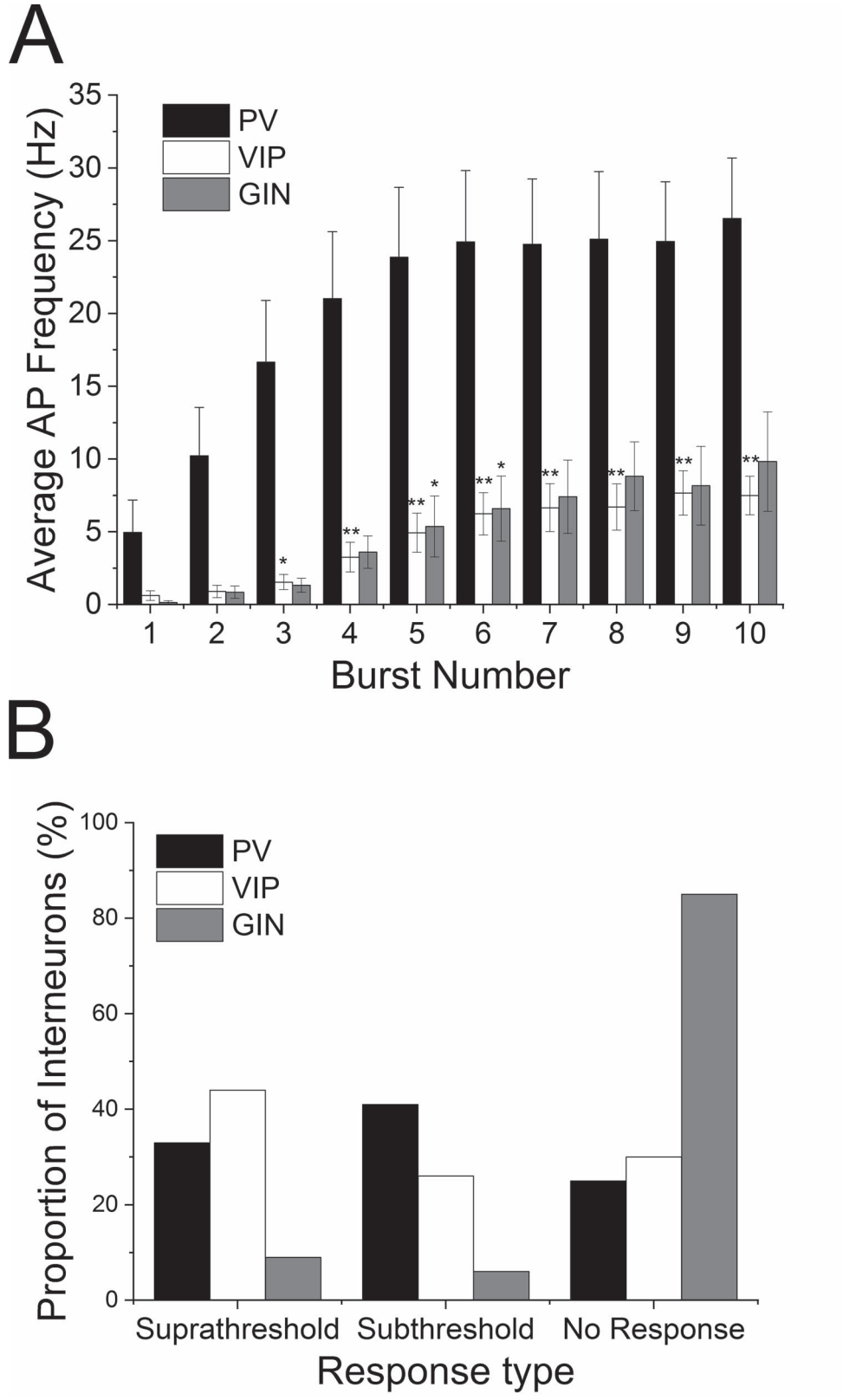

Figure 9. Parvalbumin-expressing interneurons are more excitable to alvear inputs than VIP or GIN interneurons. (*A*) Bar graph illustrating the averaged action potential firing frequency of PV (black, $n = 29$), VIP (white, $n = 14$), or GIN (gray, $n = 7$) interneurons during each burst of a 5 Hz optogenetic theta burst stimulation. (*B*) Proportion of PV (black), VIP (white) interneurons and GIN (gray) that generated suprathreshold (left), subthreshold (middle), or no response (right) in response to 5 Hz optogenetic theta burst stimulation of the alvear pathway in hippocampal CA1.

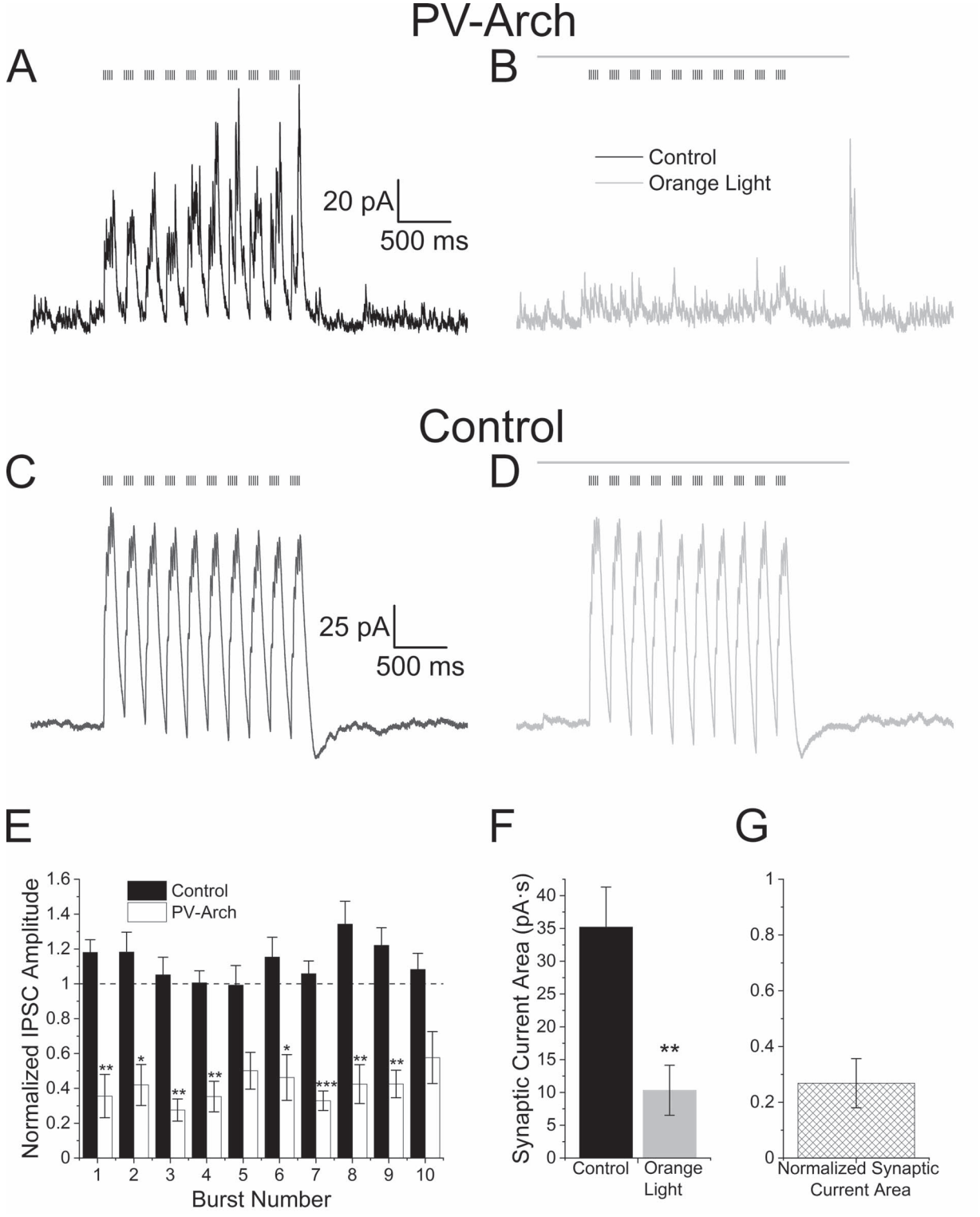

Figure 10. Suppression of PV interneuron activity inhibits alvear pathway driven disynaptic inhibitory currents in hippocampal CA1 pyramidal neurons. (*A*) 5 Hz optogenetic theta burst (black vertical lines above traces) stimulation of alvear inputs produced outward IPSCs in a voltage clamped CA1 pyramidal neuron held at +15 mV in a slice that expressed Arch-GFP in PV interneurons. (*B*) On alternating trials, an orange light pulse (gray line above traces, 3000 ms duration) was initiated 500 ms before and ended 620 ms after the theta burst stimuli, which nearly completely eliminated the outward IPSCs. (*C*) 5 Hz optogenetic theta burst (black vertical lines above traces) stimulation of alvear inputs produced outward IPSCs in a voltage clamped CA1 pyramidal neuron held at +15 mV from a slice in which Arch-GFP was not expressed in PV interneurons. (*D*) An orange light pulse (gray line above traces, 3000 ms duration) had no significant effect on the alvear input driven IPSCs in same cell shown in C. (*E*) Bar plot illustrating the normalized maximum IPSC amplitude for each burst (orange light/no orange light). Black bars (control) were measured in pyramidal cells in mice lacking Arch-GFP whereas open bars were measured in pyramidal cells in PV; Arch-GFP mice. (*F*) Bar plot illustrating the effect of orange light (gray bar) on the total current area produced by alvear pathway driven IPSCs in CA1 pyramidal neurons (control black bars). (*G*) Normalized average IPSC area produced by theta burst train in the presence of orange light.

elements in SO and not due to the potential propagation of action potentials to alvear terminals located in the SLM.

Although the timing of action potentials in individual MEC L3 projection neurons do not correlate well with population EC theta field potentials, MEC L3 projection neurons do fire coherently with their own internal theta activity (Quilichini et al. 2010; Domnisoru et al. 2013). More recently, a population of MEC L2 PCs that express calbindin have been identified that selectively project to hippocampal CA1 (Kitamura et al. 2014; Ray et al. 2014). The firing pattern of these neurons are strongly correlated with local population theta rhythms. However, it is unknown whether these MEC L2 PCs contribute to the alvear pathway. Nevertheless, theta burst stimulation of the SLM occasionally resulted in the generation of a distal apical dendritic spikes in CA1 PCs (Takahashi and Magee 2009). However, robust optogenetic theta burst stimulation of the alvear pathway in the SO did not produce suprathreshold EPSPs measured from CA1 PC somas. These data may seem to suggest that the TA pathway input is stronger than the alvear pathway in producing responses in hippocampal CA1 PCs. However, stimulation in the SLM (Takahashi and Magee 2009) would activate more than just TA synaptic terminals. SLM stimulation potentially activates alvear inputs that ultimately project to the SLM (Deller et al. 1996) as well as glutamatergic inputs that arise from the thalamic nucleus reuniens (Wouterlood et al. 1990; Dolleman–Van Der Weel and Witter 1996). Therefore, a direct comparison between the strengths of TA and alvear inputs was not possible with previous studies. Nevertheless, our studies do suggest that stimulation of SO alvear inputs were not strong enough to drive CA1 PCs to fire action potentials.

In contrast to CA1 PCs, theta burst stimulation of the MEC alvear pathway was capable of eliciting suprathreshold excitation of interneurons with cell bodies located in the SO and SP of hippocampal CA1. However, not all subtypes of interneurons were equally excited by theta burst stimulation of the alvear pathway. Interneurons expressing PV produced a higher frequency of action potentials relative to interneurons expressing VIP or GIN interneurons. Furthermore, a larger proportion of PV and VIP interneurons produced suprathreshold or subthreshold responses compared to GIN interneurons. Importantly, different subtypes of PV and VIP interneurons could produce bursts of action potential by theta burst stimulation of the alvear pathway. These responsive interneuron subtypes included PV and VIP perisomatic interneurons as well as PV bistratified and presumptive VIP interneuron-selective interneurons (Booker and Vida 2018). Furthermore, the PV suprathreshold responsive neurons could have horizontal or vertically oriented dendrites. Notably, PV interneurons have been demonstrated to produce little to no response to SLM stimulation (Milstein et al. 2015). Therefore, alvear pathway terminals in the SO appear to be capable of activating different subsets of interneurons relative to TA inputs.

PV interneurons play a crucial role in coordinating biologically relevant rhythms in populations of hippocampal principal cells (Buzsaki and Wang 2012). These rhythms include gamma and theta rhythms. Our observations that alvear theta burst stimulation produced rhythmic IPSCs in CA1 PCs is consistent with previous observations. Moreover, we have also demonstrated that theta burst stimulation of the alvear pathway can generate burst firing of PV interneurons. Importantly, optogenetic silencing of PV interneurons during alvear theta burst stimulation resulted in a greater than 50% reduction in burst IPSC amplitudes observed in CA1 PCs. Given that the largest source of theta rhythm generation arises from the EC (Buzsaki et al. 1983; Bragin et al. 1995; Kamondi et al. 1998), our data suggest that alvear excitation of PV interneurons in hippocampal CA1 may contribute to theta rhythm generation by perisomatic interneurons (Buzsaki 2002; Buzsaki and Wang 2012).

In addition to being important for normal brain function, the EC is one of the first regions in the brain to display neurodegeneration and dysfunction in Alzheimer's disease (AD) (Braak and Del Trecidi 2015). The initial pathology associated with AD is hallmarked by an accumulation of hyperphosphorylated tau protein that misfolds and eventually forms insoluble intracellular neurofibrillary tangles in EC projection neurons (Braak and Braak 1991, 1992; Braak et al. 2006; Braak and Del Trecidi 2015). Tau spreads trans-synaptically from the EC to hippocampal CA1 (stage II) and from there to other parts of the cerebrum (stages III–VI). Notably, in AD patients, tau protein has been shown to accumulate in the terminals of the alvear pathway but not the perforant path (Shukla and Bridges 2001), suggesting that the alvear input may be particularly vulnerable at early stages of the disease. Thus, our studies may provide a basis from which to examine potential changes in hippocampal network function at early stages of AD.

In conclusion, our study demonstrated that the alvear pathway from the MEC innervated both CA1 PCs and interneurons. These glutamatergic excitatory inputs were weak and incapable of activating CA1 PCs but were capable of eliciting action potentials in interneurons. However, not all interneurons were equally affected. PV-expressing interneurons were more excitable compared to VIP-expressing and GIN interneurons (a subset of O-LM interneurons). Greater than half of the feedforward inhibition in CA1 PCs produced by theta stimulation of the alvear pathway was due to the activation of PV interneurons, many of which were perisomatic. Furthermore, the subset of interneurons activated by the alvear pathway in the deep layers of hippocampal CA1 appear to be different from those activated by the TA. Therefore, our data suggests that the MEC alvear pathway primarily affects hippocampal CA1 function by driving feedforward inhibition. Furthermore, we propose that this pathway may contribute to the generation of theta rhythms.

Notes

The authors would like to thank Dr Susumu Tonegawa for generously donating the pOXR-1-Cre mice, Dr Leonardo Belluscio for donating the TRE-oChIEF-mCitrine mice, and Dr John Dempster for providing WCP electrophysiological software. *Conflict of Interest*: None declared.

Funding

National Institutes of Health (R01MH107507, R21AG055073 to A.R.M.).

References

Andersen P, Holmqvist B, Voorhoeve PE. 1966. Excitatory synapses on hippocampal apical dendrites activated by entorhinal stimulation. *Acta Physiol Scand*. 66:461–472.

Ang CW, Carlson GC, Coulter DA. 2005. Hippocampal CA1 circuitry dynamically gates direct cortical inputs preferentially at theta frequencies. *J Neurosci*. 25:9567–9580.

Bell KA, Shim H, Chen CK, McQuiston AR. 2011. Nicotinic excitatory postsynaptic potentials in hippocampal CA1 interneurons are predominantly mediated by nicotinic receptors that contain a4 and b2 subunits. *Neuropharmacology*. 61:1379–1388.

Bell LA, Bell KA, McQuiston AR. 2015. Activation of muscarinic receptors by ACh release in hippocampal CA1 depolarizes VIP but has varying effects on parvalbumin-expressing basket cells. *J Physiol*. 593:197–215.

Booker SA, Vida I. 2018. Morphological diversity and connectivity of hippocampal interneurons. *Cell Tissue Res*. 373:619–641.

Braak H, Alafuzoff I, Arzberger T, Kretzschmar H, Del Tredici K. 2006. Staging of Alzheimer disease-associated neurofibrillary pathology using paraffin sections and immunocytochemistry. *Acta Neuropathol*. 112:389–404.

Braak H, Braak E. 1991. Neuropathological stageing of Alzheimer-related changes. *Acta Neuropathol*. 82:239–259.

Braak H, Braak E. 1992. The human entorhinal cortex: normal morphology and lamina-specific pathology in various diseases. *Neurosci Res*. 15:6–31.

Braak H, Del Trecidi K. 2015. Neuroanatomy and pathology of sporadic Alzheimer's disease. *Adv Anat Embryol Cell Biol*. 215:1–162.

Bragin A, Jando G, Nadasdy Z, Hetke J, Wise K, Buzsaki G. 1995. Gamma (40–100 Hz) oscillation in the hippocampus of the behaving rat. *J Neurosci*. 15:47–60.

Buzsaki G. 2002. Theta oscillations in the hippocampus. *Neuron*. 33:325–340.

Buzsaki G, Leung LW, Vanderwolf CH. 1983. Cellular bases of hippocampal EEG in the behaving rat. *Brain Res*. 287:139–171.

Buzsaki G, Wang XJ. 2012. Mechanisms of gamma oscillations. *Annu Rev Neurosci*. 35:203–225.

Cheetham CEJ, Park U, Belluscio L. 2016. Rapid and continuous activity-dependent plasticity of olfactory sensory input. *Nat Commun*. 7:10729.

Chow BY, Han X, Dobry AS, Qian X, Chuong AS, Li M, Henninger MA, Belfort GM, Lin Y, Monahan PE *et al*. 2010. High-performance genetically targetable optical neural silencing by light-driven proton pumps. *Nature*. 463:98–102.

Colbert CM, Levy WB. 1992. Electrophysiological and pharmacological characterization of perforant path synapses in CA1: mediation by glutamate receptors. *J Neurophysiol*. 68:1–8.

Council NR. 2011. *Guide for the Care and Use of Laboratory Animals: Eighth Edition*. Washington, DC: The National Academies Press.

Deller T, Adelmann G, Nitsch R, Frotscher M. 1996. The Alvear pathway of the rat hippocampus. *Cell Tissue Res*. 286:293–303.

Dolleman-Van Der Weel MJ, Witter MP. 1996. Projections from the nucleus reuniens thalami to the entorhinal cortex, hippocampal field CA1, and the subiculum in the rat arise from different populations of neurons. *J Comp Neurol*. 364:637–650.

Domnisoru C, Kinkhabwala AA, Tank DW. 2013. Membrane potential dynamics of grid cells. *Nature*. 495:199–204.

Dvorak-Carbone H, Schuman EM. 1999. Patterned activity in stratum lacunosum moleculare inhibits CA1 pyramidal neuron firing. *J Neurophysiol*. 82:3213–3222.

Empson RM, Heinemann U. 1995a. Perforant path connections to area CA1 are predominantly inhibitory in the rat hippocampal-entorhinal cortex combined slice preparation. *Hippocampus*. 5:104–107.

Empson RM, Heinemann U. 1995b. The perforant path projection to hippocampal area CA1 in the rat hippocampal-entorhinal cortex combined slice. *J Physiol*. 484(Pt 3):707–720.

Hippenmeyer S, Vrieseling E, Sigrist M, Portmann T, Laengle C, Ladle DR, Arber S. 2005. A developmental switch in the response of DRG neurons to ETS transcription factor signaling. *PLoSBiol*. 3:e159.

Kaiser T, Ting JT, Monteiro P, Feng G. 2016. Transgenic labeling of parvalbumin-expressing neurons with tdTomato. *Neuroscience*. 321:236–245.

Kamondi A, Acsady L, Wang XJ, Buzsaki G. 1998. Theta oscillations in somata and dendrites of hippocampal pyramidal cells in vivo: activity-dependent phase-precession of action potentials. *Hippocampus*. 8:244–261.

Kitamura T, Pignatelli M, Suh J, Kohara K, Yoshiki A, Abe K, Tonegawa S. 2014. Island cells control temporal association memory. *Science*. 343:896–901.

Klausberger T, Somogyi P. 2008. Neuronal diversity and temporal dynamics: the unity of hippocampal circuit operations. *Science*. 321:53–57.

Leung LS, Roth L, Canning KJ. 1995. Entorhinal inputs to hippocampal CA1 and dentate gyrus in the rat: a current-source-density study. *J Neurophysiol*. 73:2392–2403.

Lin JY, Lin MZ, Steinbach P, Tsien RY. 2009. Characterization of engineered channelrhodopsin variants with improved properties and kinetics. *Biophys J*. 96:1803–1814.

Madisen L, Zwingman TA, Sunkin SM, Oh SW, Zariwala HA, Gu H, Ng LL, Palmiter RD, Hawrylycz MJ, Jones AR *et al*. 2010. A robust and high-throughput Cre reporting and characterization system for the whole mouse brain. *Nat Neurosci*. 13:133–140.

McQuiston AR. 2007. Effects of mu-opioid receptor modulation on GABAB receptor synaptic function in hippocampal CA1. *J Neurophysiol*. 97:2301–2311.

McQuiston AR. 2008. Layer selective presynaptic modulation of excitatory inputs to hippocampal cornu Ammon 1 by mu-opioid receptor activation. *Neuroscience*. 151: 209–221.

McQuiston AR. 2011. Mu opioid receptor activation normalizes temporo-ammonic pathway driven inhibition in hippocampal CA1. *Neuropharmacology*. 60:472–479.

Melzer S, Michael M, Caputi A, Eliava M, Fuchs EC, Whittington MA, Monyer H. 2012. Long-range-projecting GABAergic neurons modulate inhibition in hippocampus and entorhinal cortex. *Science*. 335:1506–1510.

Milstein AD, Bloss EB, Apostolides PF, Vaidya SP, Dilly GA, Zemelman BV, Magee JC. 2015. Inhibitory gating of input comparison in the CA1 microcircuit. *Neuron*. 87: 1274–1289.

Oliva AA Jr, Jiang M, Lam T, Smith KL, Swann JW. 2000. Novel hippocampal interneuronal subtypes identified using transgenic mice that express green fluorescent protein in GABAergic interneurons. *J Neurosci*. 20:3354–3368.

Paxinos G, Franklin KBJ. 2019. *Paxinos and Franklin's The Mouse Brain in Stereotaxic Coordinates*. London: Academic Press, an imprint of Elsevier.

Pelkey KA, Chittajallu R, Craig MT, Tricoire L, Wester JC, McBain CJ. 2017. Hippocampal GABAergic inhibitory interneurons. *Physiol Rev*. 97:1619–1747.

Petreanu L, Huber D, Sobczyk A, Svoboda K. 2007. Channelrhodopsin-2-assisted circuit mapping of long-range callosal projections. *Nat Neurosci*. 10:663–668.

Quilichini P, Sirota A, Buzsaki G. 2010. Intrinsic circuit organization and theta-gamma oscillation dynamics in the entorhinal cortex of the rat. *J Neurosci*. 30:11128–11142.

Ray S, Naumann R, Burgalossi A, Tang Q, Schmidt H, Brecht M. 2014. Grid-layout and theta-modulation of layer 2 pyramidal neurons in medial entorhinal cortex. *Science*. 343:891–896.

Segal M. 1972. Hippocampal unit responses to perforant path stimulation. *Exp Neurol*. 35:541–546.

Shukla C, Bridges LR. 2001. Tau, beta-amyloid and beta-amyloid precursor protein distribution in the entorhinal-hippocampal Alvear and perforant pathways in the Alzheimer's brain. *Neurosci Lett*. 303:193–197.

Soltesz I, Deschenes M. 1993. Low- and high-frequency membrane potential oscillations during theta activity in CA1 and CA3 pyramidal neurons of the rat hippocampus under ketamine-xylazine anesthesia. *J Neurophysiol*. 70:97–116.

Steward O. 1976. Topographic organization of the projections from the entorhinal area to the hippocampal formation of the rat. *J Comp Neurol*. 167:285–314.

Steward O, Scoville SA. 1976. Cells of origin of entorhinal cortical afferents to the hippocampus and fascia dentata of the rat. *J Comp Neurol*. 169:347–370.

Suh J, Rivest AJ, Nakashiba T, Tominaga T, Tonegawa S. 2011. Entorhinal cortex layer III input to the hippocampus is crucial for temporal association memory. *Science*. 334:1415–1420.

Takahashi H, Magee JC. 2009. Pathway interactions and synaptic plasticity in the dendritic tuft regions of CA1 pyramidal neurons. *Neuron*. 62:102–111.

Taniguchi H, He M, Wu P, Kim S, Paik R, Sugino K, Kvitsiani D, Fu Y, Lu J, Lin Y *et al*. 2011. A resource of Cre driver lines for genetic targeting of GABAergic neurons in cerebral cortex. *Neuron*. 71:995–1013.

Wouterlood FG, Saldana E, Witter MP. 1990. Projection from the nucleus reuniens thalami to the hippocampal region: light and electron microscopic tracing study in the rat with the anterograde tracer Phaseolus vulgaris-leucoagglutinin. *J Comp Neurol*. 296:179–203.

Yasuda M, Mayford MR. 2006. CaMKII activation in the entorhinal cortex disrupts previously encoded spatial memory. *Neuron*. 50:309–318.

Yeckel MF, Berger TW. 1990. Feedforward excitation of the hippocampus by afferents from the entorhinal cortex: redefinition of the role of the trisynaptic pathway. *Proc Natl Acad Sci USA*. 87:5832–5836.

Yeckel MF, Berger TW. 1995. Monosynaptic excitation of hippocampal CA1 pyramidal cells by afferents from the entorhinal cortex. *Hippocampus*. 5:108–114.

Zeineh MM, Palomero-Gallagher N, Axer M, Grassel D, Goubran M, Wree A, Woods R, Amunts K, Zilles K. 2017. Direct visualization and mapping of the spatial course of fiber tracts at microscopic resolution in the human hippocampus. *Cereb Cortex*. 27:1779–1794.